Mathematical Control and Related Fields
Vol. 15, No. 1, March 2025, pp. 68-100
doi:10.3934/mcrf.2023043

ROBUSTNESS OF FEEDBACK CONTROL FOR SIQR EPIDEMIC MODEL UNDER MEASUREMENT UNCERTAINTY

Summer Atkins[*1] and Michael Malisoff[1]

[1]Department of Mathematics, Louisiana State University, Baton Rouge, LA USA 70803-4918

(Communicated by Benedetto Piccoli)

Abstract. We study a model for susceptible, infected, quarantined, and recovered (SIQR) populations, in the presence of an infectious disease. The three feedback controls represent isolation, contact regulation, and vaccination. The model contains four time-varying uncertainties. One uncertainty models uncertain immigration. The other three uncertainties represent uncertainties in the measurements of state components that are used in the feedback control. We use the input-to-state stability (ISS) framework. Using a strict Lyapunov function construction method from a recent paper by H. Ito, M. Malisoff, and F. Mazenc whose uncertainties were confined to be uncertain immigration, we provide two ISS results that quantify the robustness of the feedback control, with respect to the four uncertainties. Our first theorem proves ISS of the SIQR error dynamics with all four uncertainties present in the ISS overshoot term. The error variable measures the difference between the current state of the SIQR dynamics and the prescribed endemic equilibrium. Our second theorem proves ISS where the overshoot in the ISS estimate only depends on the immigration uncertainty, and so ensures robust asymptotic stability when no immigration uncertainty is present, under a new condition on the allowable measurement uncertainties. We illustrate the effectiveness of our approach in simulations, using parameter values from the COVID-19 pandemic.

1. **Introduction.** This paper continues the development (which began in [9, 10]) of strict Lyapunov function based methods that quantify the effects of uncertainty in feedback controlled models for susceptible, infected, quarantined, and recovered individuals, called SIQR models. While [8, 9, 10] only allowed the uncertainty to be in the immigration rate into the susceptible population, here our models contain all three feedback controls and, in addition to uncertain immigration, there are measurement uncertainties in the state values that are used in its feedback controls. This models realistic scenarios having up to 20% (or more) overcounting or undercounting of susceptible, infected, or quarantined individuals, and where the disease cannot be eliminated by solely using vaccination. Undercounting and overcounting occur, e.g., from reluctance of individuals to be tested, insufficiently many test kits,

2020 *Mathematics Subject Classification.* Primary: 93D30, 93C10, 93D09; Secondary: 92D25, 34D23.

Key words and phrases. Epidemic models, quarantine, contact regulations, vaccination, Lyapunov functions, robustness.

The first author is supported by US National Science Foundation Division of Mathematical Sciences Grant 2009659.

*Corresponding author: Summer Atkins.

or false positives or false negatives arising from deficiencies in tests early in a pandemic. Unlike the immigration uncertainty which is an additive uncertainty on the growth rate of the susceptible population, the measurement uncertainties multiply the states in the controls, and so call for the novel methods below involving a new equal signs condition; see Remark 3.2 in Section 3 below.

As noted in [9, 10], strict Lyapunov functions are a valuable alternative to traditional solutions to disease control problems, which often entail linearization. Since linearization only implies convergence properties in a small enough region around the setpoint, Lyapunov functions are often used to obtain global convergence results, i.e., for all componentwise positive initial state vectors. Nonstrict Lyapunov functions are often used in conjunction with LaSalle invariance to obtain global convergence [13]. Nonstrict means that the time derivative of the Lyapunov function at all points outside the prescribed equilibrium is nonpositive (but not necessarily negative), while the strict Lyapunov function condition [18] calls for this time derivative to be negative at each point outside the equilibrium. This strictness makes it possible to quantify the effects of uncertainty, which contrasts with nonstrict Lyapunov functions which are not amenable to robustness analysis [5, 6, 7]. Other approaches for population models include removal of variables and adding state space restrictions [4, 14, 15, 16, 23, 24, 25], leading to Lyapunov functions in a restricted domain or the assumption of a constant population. Such alternative methods are usually not amenable to proving robustness properties in the input-to-state stability (ISS) sense, which plays an essential role in robustness analysis [13, 21]. Throughout this work, the uncertainties are unknown locally bounded piecewise continuous functions.

The ISS property is a generalization of asymptotic stability that quantifies the effects of uncertainties in overshoot terms; see the definition of ISS below. In this paper, we prove two ISS theorems for SIQR models with uncertain immigration rates and uncertain measurements of the susceptible, infected, and quarantined individuals in the feedback controls, whose significance can be summarized as follows:

1. Our first theorem provides an overshoot term that depends on all four uncertainties, and the result is semiglobal, because it provides a different ISS estimate for each compact set of initial states and each compact set of admissible values for the uncertainties, and it computes rates of exponential decay for the asymptotically decaying term in the ISS upper bound.
2. By contrast, our second theorem yields a global ISS estimate in which the overshoot only depends on the uncertainty in the immigration rate. Hence, when the immigration uncertainty is zero, we obtain robust global asymptotic stability, where the same global asymptotic stability estimate holds regardless of the initial state and regardless of the specific measurement uncertainties. This calls for the measurement uncertainties to satisfy a set of inequalities involving the current state, so the set of admissible measurement uncertainties changes over time. This is a significant departure from prior robustness analyses whose uncertainty bounds were independent of the state.

In our second theorem, the set of inequalities quantifies the requirement that more measurement uncertainty is allowed when the state is far from the endemic equilibrium, as compared with times when the state is closer to the equilibrium. Also, as noted in [10], our approach is a significant departure from optimal control approaches. While optimal control can be useful for policy makers who may not always express their goals in a mathematical way, we believe that our approach is

a useful complementary alternative that quantifies the effects of uncertainty in the important ISS framework that facilitates comparing the effects of different feedback control parameters, without incurring the cost of real-time updates that would rely on numerical computations and data storage. It also differs from [1, 2, 3, 20], which either do not involve feedback control or do not consider measurement uncertainty, and so are not germane to or overlapping with this work.

We use the following definitions and notation. We use $|f|_J$ to denote the usual sup norm of a function f over a subset J of its domain, $|f|_\infty$ is the sup norm over its entire domain, and $|\cdot|$ is the usual Euclidean norm. Let $\mathcal{K}$ denote the set of all strictly increasing continuous functions $\alpha : [0, +\infty) \to [0, +\infty)$ such that $\alpha(0) = 0$; if, in addition, α is unbounded, then we say that α is of class $\mathcal{K}_\infty$. We say that a continuous function $\Phi : [0, +\infty) \times [0, +\infty) \to [0, +\infty)$ is of class $\mathcal{KL}$ provided for each fixed $s > 0$, the function $\Phi(\cdot, s)$ belongs to class $\mathcal{K}$, and for each fixed $r \geq 0$, the function $\Phi(r, \cdot)$ is non-increasing and $\Phi(r, s) \to 0$ as $s \to +\infty$, and 0 denotes the zero vector. A system of the form $\dot{x}(t) = F(x(t), \varepsilon(t))$ with a state space $\mathcal{X} \subseteq \mathbb{R}^n$ satisfying $F(0, 0) = 0$ is called input-to-state stable (also abbreviated as ISS) [13] on $\mathcal{X}$ with respect to a disturbance set $\mathcal{E}$ provided: There are $\Phi \in \mathcal{KL}$ and $\Gamma \in \mathcal{K}_\infty$ such that for each initial state $x(0) \in \mathcal{X}$ and each locally bounded piecewise continuous function ε taking all of its values in $\mathcal{E}$, the unique corresponding solution $x : [0, +\infty) \to \mathcal{X}$ of the dynamics satisfies $|x(t)| \leq \Phi(|x(0)|, t) + \Gamma(|\varepsilon|_{[0,t]})$ for all $t \geq 0$. We use the function $\mathrm{sgn} : \mathbb{R} \to \{-1, 0, 1\}$ which is defined by $\mathrm{sgn}(0) = 0$ and $\mathrm{sgn}(x) = -1$ (resp., 1) for all $x < 0$ (resp., $x > 0$).

2. **SIQR model and strict Lyapunov function from [10].** We review the SIQR model and strict Lyapunov function from [10] in this section, to provide the essential equations that we need in later sections and make our work self-contained. As in [10], we study the dynamics

$$\begin{array}{rcl} \dot{S}(t) & = & B + \epsilon(t) - \rho(t)S(t) - \mu S(t) - \beta(t)I(t)S(t), \\ \dot{I}(t) & = & \beta(t)I(t)S(t) - (\gamma + \nu(t) + \mu)I(t), \\ \dot{Q}(t) & = & \nu(t)I(t) - (\tau + \mu)Q(t), \\ \dot{R}(t) & = & \gamma I(t) + \tau Q(t) - \mu R(t) + \rho(t)S(t), \end{array} \tag{1}$$

where the positive real valued state variables S, I, Q, and R are numbers of susceptible, infected, quarantined, and recovered individuals, respectively [4, 12, 19], and the constant $B > 0$ is the immigration rate that includes newborn. The unknown locally bounded piecewise continuous function ϵ represents the immigration perturbation, and is assumed to take all of its values in the perturbation set $\mathcal{P} = (-B, +\infty)$.

The non-negative-valued function β combines the rate of disease contact and transmission. The positive constants μ and γ are the rates of non-associated mortality rate and recovery from the disease, respectively. The non-negative-valued functions ρ and ν are the vaccination rate and the rate at which infected individuals are isolated from quarantine, respectively. The positive constant τ is the reciprocal of the average time spent in isolation, and ρ is the amount of vaccine administration and the reciprocal of the average time to acquire immunity. The positivity of the constants implies that with our choice $\mathcal{D} = (0, +\infty)^4$ of the state space for (1), each component of (1) is positive for all $t \geq 0$ for each initial state $(S(0), I(0), Q(0), R(0)) \in \mathcal{D}$. We take ρ, ν, and β as feedback controls, which depend on time t through their dependence on S, I, and Q.

To specify the desired endemic equilibrium, the error dynamics, and the class of controls, we use

$$\rho(t) = \hat{\rho} + u_V(t),\ \nu(t) = \hat{\nu} + u_I(t),\ \text{and}\ \beta(t) = \hat{\beta} + u_C(t), \tag{2}$$

for positive constants $\hat{\rho}$, $\hat{\nu}$, and $\hat{\beta}$ that represent nominal rates, where u_V, u_I, and u_C will be specified such that $u_V(t) \in [-\hat{\rho}, +\infty)$, $u_I(t) \in [-\hat{\nu}, +\infty)$, and $u_C(t) \in [-\hat{\beta}, 0]$ for all $t \geq 0$. We use the constants

$$\lambda = \gamma + \hat{\nu} + \mu,\ \chi = \hat{\rho} + \mu,\ \text{and}\ \hat{R}_0 = \tfrac{\hat{\beta}B}{(\hat{\rho}+\mu)(\gamma+\hat{\nu}+\mu)},$$

where $\hat{R}_0$ is called the basic reproduction number and is assumed to satisfy $\hat{R}_0 > 1$, which implies that the nominal vaccination rate $\hat{\rho}$ is not large enough relative to the natural disease transmission rate $\hat{\beta}$ to eliminate the disease. It also implies that, when ϵ is the zero function and $u_V = u_I = u_C = 0$, simple calculations show that (1) has the componentwise positive equilibrium $X_\star = (S_\star, I_\star, Q_\star, R_\star)$ whose components are defined by

$$\begin{array}{l}(S_\star, I_\star, Q_\star, R_\star) = \\ \left(\frac{\lambda}{\hat{\beta}},\ \frac{B}{\lambda} - \frac{\chi}{\hat{\beta}},\ \frac{\hat{\nu}}{\tau+\mu}\left(\frac{B}{\lambda} - \frac{\chi}{\hat{\beta}}\right),\ \frac{1}{\mu}\left[\left(\gamma + \frac{\tau\hat{\nu}}{\tau+\mu}\right)\left(\frac{B}{\lambda} - \frac{\chi}{\hat{\beta}}\right) + \frac{\hat{\rho}\lambda}{\hat{\beta}}\right]\right).\end{array}$$

For any constant $\underline{\beta} \in [0, \hat{\beta}]$ and nonnegative constants ω_V, ω_I, and ω_C, [10] used the feedback controls

$$\begin{array}{rcl} u_V(t) &=& f_V(S(t), I(t)) = \max\{-\hat{\rho},\ \omega_V H_1(S(t), I(t))\} \\ u_I(t) &=& f_I(S(t), I(t), Q(t)) = \max\{-\hat{\nu},\ \omega_I(H_2(S(t), I(t)) - I(t)H_3(Q(t)))\} \\ u_C(t) &=& f_C(S(t), I(t)) \\ &=& \max\left\{\underline{\beta} - \hat{\beta},\ \min\{0,\ \omega_C S(t)(I(t)H_1(S(t), I(t)) - H_2(S(t), I(t)))\}\right\} \end{array} \tag{3}$$

using the functions and error variables

$$\begin{array}{rcl} H_1(S, I) &=& (1+c)\tilde{S} + c\left(\frac{\hat{\rho}+\mu}{\hat{\beta}} \ln \frac{I}{I_\star} + \tilde{I}\right), \\ H_2(S, I) &=& c\left(\tilde{S} + \frac{\hat{\rho}+\mu}{\hat{\beta}} \ln \frac{I}{I_\star} + \tilde{I}\right)\left(\frac{\hat{\rho}+\mu}{\hat{\beta}} + I\right) + \frac{(c+1)(\gamma+\hat{\nu}+\mu)}{\hat{\beta}}\tilde{I},\ \text{and} \\ H_3(Q) &=& c_\Diamond \tilde{Q},\ \text{where}\ \tilde{S} = S - S_\star,\ \tilde{I} = I - I_\star,\ \text{and}\ \tilde{Q} = Q - Q_\star \end{array} \tag{4}$$

for any positive constant $c > 0$ and any constant $c_\Diamond \in (0, 2\overline{c}_\Diamond)$ where

$$\overline{c}_\Diamond = \tfrac{(\tau+\mu)c\lambda}{\hat{\nu}^2}, \tag{5}$$

and where the preceding constants are used to tune the controls. Then $H_1(S_\star, I_\star) = 0$, $H_2(S_\star, I_\star) = 0$, and $H_3(Q_\star) = 0$. Also as in [10], we study the dynamics for the transformed error dynamics, using $\tilde{\xi} = \ln(I/I_\star)$, $\psi_\star = \lambda I_\star$, $\xi_\star = \ln(I_\star)$, $\xi = \ln(I)$, and $\tilde{R} = R - R_*$, which give $\tilde{\xi} = \xi - \xi_\star$. Then (4) transforms (1) into [10]

$$\begin{array}{rcl} \dot{\tilde{S}}(t) &=& \epsilon(t) - \left(\chi + \hat{\beta}e^{\tilde{\xi}(t)+\xi_\star}\right)\tilde{S}(t) + \psi_\star\left(1 - e^{\tilde{\xi}(t)}\right) - u_V(t)S(t) \\ && -u_C(t)e^{\xi(t)}S(t), \\ \dot{\tilde{\xi}}(t) &=& \hat{\beta}\tilde{S}(t) - u_I(t) + u_C(t)S(t), \\ \dot{\tilde{Q}}(t) &=& \hat{\nu}e^{\xi_\star}(e^{\tilde{\xi}(t)} - 1) - (\tau+\mu)\tilde{Q}(t) + u_I(t)e^{\xi(t)}, \\ \dot{\tilde{R}}(t) &=& \gamma e^{\xi_\star}(e^{\tilde{\xi}(t)} - 1) + \tau\tilde{Q}(t) - \mu\tilde{R}(t) + \hat{\rho}\tilde{S}(t) + u_V(t)S(t) \end{array} \tag{6}$$

which are called the transformed error dynamics, and which are defined on the state space $\tilde{\mathcal{D}} = (-S_\star, +\infty) \times \mathbb{R} \times (-Q_\star, +\infty) \times (-R_\star, +\infty)$. The ISS analysis in [10] is performed for (6), using the ISS Lyapunov function

$$\begin{array}{l} V(\tilde{S},\tilde{\xi},\tilde{Q},\tilde{R}) = U(\tilde{S},\tilde{\xi},\tilde{Q}) + W(\tilde{S},\tilde{\xi},\tilde{Q},\tilde{R}), \text{ where} \\ U(\tilde{S},\tilde{\xi},\tilde{Q}) = \frac{1}{2}\tilde{S}^2 + \frac{c}{2}\left[\tilde{S} + \frac{\chi}{\hat{\beta}}\tilde{\xi} + I_\star\left(e^{\tilde{\xi}} - 1\right)\right]^2 + \frac{(c+1)\psi_\star}{\hat{\beta}}\left(e^{\tilde{\xi}} - 1 - \tilde{\xi}\right) \\ \qquad\qquad + \frac{c_\diamond}{2}\tilde{Q}^2, \\ \text{and } W(\tilde{S},\tilde{\xi},\tilde{Q},\tilde{R}) = \frac{g}{2}\left[\tilde{S} + I_\star\left(e^{\tilde{\xi}} - 1\right) + \tilde{Q} + \tilde{R}\right]^2, \end{array} \tag{7}$$

where $g > 0$ is another tuning constant. Although not stated in [10], the proof of this lemma follows from the proofs in [10] and is reported here because it will be essential for future sections below:

Lemma 2.1. *Let $c > 0$, $g > 0$, $c_\diamond \in (0, 2\overline{c}_\diamond)$, $\underline{\beta} \in [0, \hat{\beta}]$, and the nonnegative values ω_V, ω_I, and ω_C be given constants, and choose the functions α and σ and the constants k_i for $i = 1, 2, 3, 4$ that are defined by*

$$\begin{array}{l} \alpha(r) = \min\left\{\frac{1}{2}, 1 - \sqrt{\frac{c_\diamond}{2\overline{c}_\diamond}}\right\}\left[\sqrt{k_4 + \min\left\{1/k_3, 4\sqrt{k_4}\mu\right\} r} - \sqrt{k_4}\right], \\ \sigma(r) = \left[\frac{\ln(2)c\chi}{\hat{\beta}} + cI_\star\right] r + \left[\frac{(1+c)^2}{2\chi} + \frac{g}{2\mu}\right] r^2, \\ k_1 = \max\left\{\frac{1+2c}{\chi}, \frac{2}{c\psi_\star I_\star}\left[2cI_\star^2 + \frac{(c+1)\psi_\star}{2\hat{\beta}}\right]\right\}, \\ k_2 = k_1 + \left(\frac{4c\chi^2}{\hat{\beta}} + (c+1)\psi_\star\right)\frac{4}{c\psi_\star\left(2\chi + \hat{\beta}I_\star\right)},\ k_3 = \left(\frac{2c\chi^2}{\hat{\beta}} + \frac{(c+1)\psi_\star}{2}\right)\frac{16\hat{\beta}}{c^2\psi_\star^2\chi^2}, \\ \text{and } k_4 = \frac{k_2^2}{4k_3^2}. \end{array} \tag{8}$$

Then, for any piecewise continuous locally bounded time-varying functions u_V, u_I, and u_C, the time derivative of the function V in (7) along all solutions of (6) satisfies

$$\begin{array}{rcl} \dot{V}(t) & \leq & -\alpha(V(\tilde{S}(t),\tilde{\xi}(t),\tilde{Q}(t),\tilde{R}(t))) - S(t)H_1(S(t),I(t))u_V(t) \\ & & + \big(I(t)H_3(Q(t)) - H_2(S(t),I(t))\big)u_I(t) \\ & & + S(t)\big(H_2(S(t),I(t)) - I(t)H_1(S(t),I(t))\big)u_C(t) + \sigma(|\epsilon(t)|) \end{array} \tag{9}$$

for all $t \geq 0$ and all piecewise continuous functions $\epsilon : [0, +\infty) \to [-\psi_*/4, \psi_*/4] \cap (-B, +\infty)$. □

Since α and σ are of class $\mathcal{K}_\infty$, (9) implies that V is an ISS Lyapunov function for the closed loop dynamics with the controls (3), because as noted in [10], these choices of the controls imply that $\dot{V}(t) \leq -\alpha(V(\tilde{S}(t),\tilde{\xi}(t),\tilde{Q}(t),\tilde{R}(t))) + \sigma(|\epsilon(t)|)$ for all $t \geq 0$, which implies the required ISS property when no measurement uncertainties are present. We next provide conditions under which V continues to provide ISS when measurement uncertainties Δ_S, Δ_I, and Δ_Q are also present.

3. Exponential ISS result.

This paper shares the goal of [10] of deriving formulas for feedback controls that achieve ISS of the error system (6). This will imply convergence of the states to desired values with an overshoot depending on the uncertainty. However, unlike [10] where the only uncertainty is ϵ, here the uncertainty is valued in $\mathbb{R}^4$, because the uncertainties also include $1 - \Delta_S(t)$, $\ln(\Delta_I)$ and $1 - \Delta_Q(t)$, where Δ_S, Δ_I, and Δ_Q are positive valued multiplicative uncertainties multiplying the corresponding values of S, I, and Q in the feedback controls, to model measurement uncertainty. This produces the vector of uncertainties $\epsilon^\sharp$ that is defined by $\epsilon^\sharp(t) = (\epsilon(t), 1 - \Delta_S(t), \ln(\Delta_I), 1 - \Delta_Q(t))$. The justification for this choice of $\epsilon^\sharp$ (instead of $(\epsilon(t), \Delta_S(t), \Delta_I(t), \Delta_Q(t))$) is that ISS requires the vector of uncertainties to take the value 0 at all times when no uncertainty is present, which in our case occurs exactly when $\epsilon(t) = 0$ and $\Delta_S(t) = \Delta_I(t) = \Delta_Q(t) = 1$. Also, we treat Δ_I differently from Δ_S and Δ_Q through the use of the ln to match the

logarithmic transformation $\xi = \ln(I)$ in (6). There is no measurement uncertainty Δ_R, because R will not appear in our feedback controls.

Hence, to account for the fact that the exact measurements $S(t)$, $I(t)$, and $Q(t)$ in (3) might not be available in practice, our controls in this and the next section will instead be

$$\begin{array}{rcl} u_V &=& \max\{-\hat{\rho},\, \omega_V H_1(\Delta_S S, \Delta_I I)\}\,, \\ u_I &=& \max\{-\hat{\nu},\, \omega_I (H_2(\Delta_S S, \Delta_I I) - \Delta_I I H_3(\Delta_Q Q))\}\,, \text{ and} \\ u_C &=& \max\{\underline{\beta} - \hat{\beta},\, \min\{0,\, \omega_C \Delta_S S(\Delta_I I H_1(\Delta_S S, \Delta_I I) - H_2(\Delta_S S, \Delta_I I))\}\} \end{array} \tag{10}$$

instead of (3), in terms of the above constants and the H_i's in (4). Our first result is as follows where $\tilde{S}$, $\tilde{I}$, $\tilde{Q}$, $\tilde{R}$, and V are from Section 2 as before, and the term exponential refers to the fact that the decaying function in the ISS estimate (11) has the form $\Phi(s,t) = b_1 s e^{-rt}$ for positive constants b_1 and r:

Theorem 3.1. *For each compact neighborhood $\mathcal{C}_0 \subseteq (-S_*, +\infty) \times (-I_*, +\infty) \times (-Q_*, +\infty) \times (-R_*, +\infty)$ of 0, each compact set $\mathcal{D}_0 \subseteq (-B, +\infty) \times (-\infty, 1) \times \mathbb{R} \times (-\infty, 1)$, each set of positive constants $\hat{\rho}$, $\hat{\nu}$, $\hat{\beta}$, c, ω_V, ω_I, and ω_C, and each constant $\underline{\beta} \in [0, \hat{\beta})$, we can construct positive constants b_1, b_2, and r such that for all solutions $(S(t), I(t), Q(t), R(t))$ of the SIQR dynamics (1) in closed loop with the controls (10) having initial states $(\tilde{S}(0), \tilde{I}(0), \tilde{Q}(0), \tilde{R}(0))$ in $\mathcal{C}_0$ and for all piecewise continuous bounded functions $\epsilon : [0, +\infty) \to (-B, +\infty)$, $\Delta_S : [0, +\infty) \to (0, +\infty)$, $\Delta_I : [0, +\infty) \to (0, +\infty)$, and $\Delta_Q : [0, +\infty) \to (0, +\infty)$ satisfying $(\epsilon(t), 1 - \Delta_S(t), \ln(\Delta_I(t)), 1 - \Delta_Q(t)) \in \mathcal{D}_0$ for all $t \geq 0$, the corresponding solutions $(\tilde{S}, \tilde{I}, \tilde{Q}, \tilde{R}) : [0, +\infty) \to \mathbb{R}^4$ satisfy*

$$\begin{array}{l} |(\tilde{S}(t), \tilde{I}(t), \tilde{Q}(t), \tilde{R}(t))| \leq b_1 |(\tilde{S}(0), \tilde{I}(0), \tilde{Q}(0), \tilde{R}(0))| e^{-rt} \\ + b_2 \left(|\epsilon|_{[0,t]} + \sqrt{|\epsilon|_{[0,t]} + |\epsilon|^2_{[0,t]} + |1 - \Delta_S|_{[0,t]} + |\ln(\Delta_I)|_{[0,t]} + |1 - \Delta_Q|_{[0,t]}} \right) \end{array} \tag{11}$$

for all $t \geq 0$.

Proof. The proof has three parts. First, we obtain bounds on the differences between values of terms in the controls (10) and the values of corresponding terms in the controls (3). Then, we use the bounds from the first part to prove that the strict Lyapunov function V from (7) satisfies a suitable ISS Lyapunov function decay conditions for the transformed SIQR error dynamics in the variable $\tilde{x} = (\tilde{S}, \tilde{\xi}, \tilde{Q}, \tilde{R})$ where $\tilde{\xi} = \ln(I/I_*)$, which will produce an ISS estimate in the variable $\tilde{x}$ when $|\epsilon|_\infty \leq \psi_*/4$. In the third part, we convert the ISS estimate in the variable $\tilde{x}$ into the required ISS estimate in the variable $\tilde{X} = (\tilde{S}, \tilde{I}, \tilde{Q}, \tilde{R})$.

First Part. Fix $\mathcal{C}_0$, $\mathcal{D}_0$, and constants satisfying the requirements of the theorem. We can find a compact set $\mathcal{C}_1$ such that all solutions $(S, I, Q, R) : [0, +\infty) \to (0, +\infty)^4$ of the SIQR dynamics with the controls (10) for all choices of the perturbation $\epsilon^\sharp(t) = (\epsilon(t), 1 - \Delta_S(t), \ln(\Delta_I(t)), 1 - \Delta_Q(t))$ that are valued in $\mathcal{D}_0$ and all initial states that satisfy $(\tilde{S}(0), \tilde{I}(0), \tilde{Q}(0), \tilde{R}(0)) \in \mathcal{C}_0$ also satisfy: $(S(t), I(t), Q(t), R(t)) \in \mathcal{C}_1$ for all $t \geq 0$. This is because the structure of the SIQR dynamics (1) gives $\dot{S}(t) + \dot{I}(t) + \dot{Q}(t) + \dot{R}(t) = -\mu(S(t) + I(t) + Q(t) + R(t)) + B + \epsilon(t)$ and so also $S(t) + I(t) + Q(t) + R(t) \leq e^{-\mu t}(S(0) + I(0) + Q(0) + R(0)) + (B + |\epsilon|_{[0,t]})/\mu$ for all $t \geq 0$ (using the integrating factor $e^{\mu t}$), so we can choose $\mathcal{C}_1 = \cup_{z \in \mathcal{C}_0} \{x \in [0, +\infty)^4 : x_1 + x_2 + x_3 + x_4 \leq z_1 + z_2 + z_3 + z_4 + S_* + I_* + Q_* + R_* + (B + \bar{\epsilon})/\mu\}$, where $\bar{\epsilon} = \max\{|d_1| : \text{there exist } (d_2, d_3, d_4) \text{ such that } (d_1, d_2, d_3, d_4) \in \mathcal{D}_0\}$. Fixing any solution and $\epsilon^\sharp$ satisfying the preceding requirements, set $\Delta_\xi = \ln(\Delta_I)$, $J_1(S, I) =$

$H_1(S,I)$, $J_2(S,I,Q) = H_2(S,I) - IH_3(Q)$, and $J_3(S,I) = S(IH_1(S,I) - H_2(S,I))$ in terms of our formulas (4) for H_1, H_2, and H_3, so our controls (10) are

$$\begin{array}{l} u_V = \max\{-\hat{\rho}, \omega_V J_1(\Delta_S S, \Delta_I I)\},\ u_I = \max\left\{-\hat{\nu},\ \omega_I J_2(\Delta_S S, \Delta_I I, \Delta_Q Q)\right\}, \\ \text{and } u_C = \max\{\underline{\beta} - \hat{\beta},\ \min\{0,\ \omega_C J_3(\Delta_S S, \Delta_I I)\}\}. \end{array} \tag{12}$$

Then we can use our formulas for H_1, H_2, and H_3 to check that the preceding functions satisfy

$$\begin{array}{rcl} J_1(\Delta_S S, \Delta_I I) & = & J_1(S,I) + (c+1)(\Delta_S - 1)S \\ & & +c\left[\frac{\hat{\rho}+\mu}{\hat{\beta}}\Delta_\xi + (\Delta_I - 1)I\right], \\ J_2(\Delta_S S, \Delta_I I, \Delta_Q Q) & = & J_2(S,I,Q) + c\Big((\Delta_S - 1)S + \frac{\hat{\rho}+\mu}{\hat{\beta}}\Delta_\xi \\ & & +(\Delta_I - 1)I\Big)\left(\frac{\hat{\rho}+\mu}{\hat{\beta}} + \Delta_I I\right) \\ & & +c\left(\tilde{S} + \frac{\hat{\rho}+\mu}{\hat{\beta}}\ln\left(\frac{I}{I_*}\right) + \tilde{I}\right)(\Delta_I - 1)I \\ & & +\frac{(c+1)(\gamma+\hat{\nu}+\mu)}{\hat{\beta}}(\Delta_I - 1)I \\ & & -(\Delta_I - 1)Ic_\diamondsuit(\Delta_Q Q - Q_*) - Ic_\diamondsuit(\Delta_Q - 1)Q, \end{array} \tag{13}$$

and

$$\begin{array}{rcl} J_3(\Delta_S S, \Delta_I I) & = & J_3(S,I) + (\Delta_S - 1)S\Big[(\Delta_S S - S_*)\Delta_I I \\ & & -c\left\{\Delta_S S - S_* + \frac{\hat{\rho}+\mu}{\hat{\beta}}\left[\ln\left(\frac{I}{I_*}\right) + \Delta_\xi\right] + \Delta_I I - I_*\right\}\frac{\hat{\rho}+\mu}{\hat{\beta}} \\ & & -\frac{(c+1)(\gamma+\hat{\nu}+\mu)}{\hat{\beta}}(\Delta_I I - I_*)\Big] + S\Big[(\Delta_S - 1)S\Delta_I I \\ & & +\tilde{S}(\Delta_I - 1)I - c\left((\Delta_S - 1)S + \frac{\hat{\rho}+\mu}{\hat{\beta}}\Delta_\xi + (\Delta_I - 1)I\right)\frac{\hat{\rho}+\mu}{\hat{\beta}} \\ & & -\frac{(c+1)(\gamma+\hat{\nu}+\mu)}{\hat{\beta}}(\Delta_I - 1)I\Big], \end{array} \tag{14}$$

using the formula $f_a g_a - f_b g_b = (f_a - f_b)g_a + f_b(g_a - g_b)$ for suitable functions f_a and g_a (which contain the disturbance terms Δ_S, Δ_I, and Δ_Q) and suitable functions f_b and g_b (which do not contain the disturbance terms), and where (14) used the fact that our formulas for H_1 and H_2 in (4) give

$$\begin{array}{l} IH_1(S,I) - H_2(S,I) = \\ \tilde{S}I - c\left(\tilde{S} + \frac{\rho+\mu}{\hat{\beta}}\ln\left(\frac{I}{I_*}\right) + \tilde{I}\right)\frac{\hat{\rho}+\mu}{\hat{\beta}} - \frac{(c+1)(\gamma+\hat{\nu}+\mu)}{\hat{\beta}}\tilde{I} \end{array} \tag{15}$$

and the fact that if we set $\mathcal{G}(S,I) = IH_1(S,I) - H_2(S,I)$, then $J_3(S,I) = S\mathcal{G}(S,I)$ and so also $J_3(\Delta_S S, \Delta_I I) - J_3(S,I) = (\Delta_S - 1)S\mathcal{G}(\Delta_S S, \Delta_I I) + S(\mathcal{G}(\Delta_S S, \Delta_I I) - \mathcal{G}(S,I))$. Also, by the compactness of $\mathcal{D}_0$ and (15), we can find a constant $L_* \geq 1$ such that $|\Delta_I - 1| = |e^{\Delta_\xi} - 1| \leq L_*|\Delta_\xi|$ along all disturbance values that satisfy the assumptions of the theorem. Therefore, if we set $\overline{\mathcal{C}} = \max\{|x| : x \in \mathcal{C}_1\}$ (which exists because $\mathcal{C}_1$ is compact), then we can use the first equality of (13) to get

$$|J_1(\Delta_S S, \Delta_I I) - J_1(S,I)| \leq \left\{(1 + c(1 + L_*))\overline{\mathcal{C}} + c\frac{\hat{\rho}+\mu}{\hat{\beta}}\right\}|(\Delta_S - 1, \Delta_\xi)|. \tag{16}$$

Also, by the compactness of $\mathcal{C}_1$ and $\mathcal{D}_0$ and the formula $J_3(S,I) = S\mathcal{G}(S,I)$ and the positiveness of the model parameters, we can find a constant $\xi_0 > 0$ such that $J_1(\Delta_S S, \Delta_I I) < 0$, $J_1(S,I) < 0$, $J_2(\Delta_S S, \Delta_I I, \Delta_Q Q) < 0$, $J_2(S,I,Q) < 0$, $J_3(\Delta_S S, \Delta_I I) > 0$, and $J_3(S,I) > 0$ all hold for all $(S,I,Q,R) \in \mathcal{C}_1$ and all $(\Delta_S, \Delta_I, \Delta_Q)$ such that $\ln(I) = \xi < -\xi_0$ and such that $\epsilon^\sharp \in \mathcal{D}_0$. We fix a ξ_0

satisfying the preceding requirements in the rest of the proof, and any constant $\bar{d}$ such that $\bar{d} \geq \max\{|\Delta_S|_\infty, |\Delta_I|_\infty, |\Delta_Q|_\infty, |\Delta_\xi|_\infty\}$ for all disturbance functions that satisfy the assumptions of the theorem (which exists because of the compactness of $\mathcal{D}_0$). It follows from (13)-(14) that

$$\begin{aligned}|J_2(\Delta_S S, \Delta_I I, \Delta_Q Q) - J_2(S,I,Q)| \quad \leq \quad & \Big\{ c\left[\overline{\mathcal{C}}(1+L_*) + \tfrac{\hat{\rho}+\mu}{\hat{\beta}}\right]\left[\tfrac{\hat{\rho}+\mu}{\hat{\beta}} + \bar{d}\overline{\mathcal{C}}\right] \\ & + \tfrac{(c+1)(\gamma+\hat{\nu}+\mu)\overline{\mathcal{C}}}{\hat{\beta}} L_* \\ & + c\Big(\overline{\mathcal{C}} + S_* + \tfrac{\hat{\rho}+\mu}{\hat{\beta}} \max\{\xi_0, |\ln(\overline{\mathcal{C}})|\} \\ & + |\ln(I_*)| + \overline{\mathcal{C}} + I_*\Big) L_* \overline{\mathcal{C}} \\ & + L_* \overline{\mathcal{C}} c_\Diamond (\bar{d}\overline{\mathcal{C}} + Q_*) + \overline{\mathcal{C}}^2 c_\Diamond \Big\} \\ & \times |(\Delta_S - 1, \Delta_\xi, \Delta_Q - 1)| \quad \text{and}\end{aligned} \tag{17}$$

$$\begin{aligned}|J_3(\Delta_S S, \Delta_I I) - J_3(S,I)| \quad \leq \quad & \Big\{ \overline{\mathcal{C}}\Big[(\bar{d}\overline{\mathcal{C}} + S_*)\bar{d}\overline{\mathcal{C}} + c\left(\bar{d}\overline{\mathcal{C}} + S_*\right. \\ & + \tfrac{\hat{\rho}+\mu}{\hat{\beta}}\left[\max\{\xi_0, |\ln(\overline{\mathcal{C}})|\} + |\ln(I_*)| + \bar{d}\right] \\ & \left. + \bar{d}\overline{\mathcal{C}} + I_*\right)\tfrac{\hat{\rho}+\mu}{\hat{\beta}} + \tfrac{(c+1)(\gamma+\hat{\nu}+\mu)}{\hat{\beta}}(\bar{d}\overline{\mathcal{C}} + I_*)\Big] \\ & + \overline{\mathcal{C}}\Big[\overline{\mathcal{C}}^2 \bar{d} + (\overline{\mathcal{C}} + S_*)\overline{\mathcal{C}} L_* \\ & + c\Big(\overline{\mathcal{C}} + \tfrac{\hat{\rho}+\mu}{\hat{\beta}} + L_*\overline{\mathcal{C}}\Big)\tfrac{\hat{\rho}+\mu}{\hat{\beta}} \\ & + \tfrac{(c+1)(\gamma+\hat{\nu}+\mu)}{\hat{\beta}}\overline{\mathcal{C}} L_*\Big]\Big\} |(\Delta_S - 1, \Delta_\xi)|\end{aligned} \tag{18}$$

for all $(S,I,Q,R) \in \mathcal{C}_1$ such that $\xi \geq -\xi_0$ and all $(\Delta_S, \Delta_I, \Delta_Q)$ satisfying the preceding requirements, where the $|\Delta_\xi|_\infty$ in the max that we used to define the lower bound for $\bar{d}$ was needed to bound the Δ_ξ in the second line of (14). We let $\bar{J}_i$ denote the quantity in curly braces in (16), (17), and (18) that multiplies either $|(\Delta_S - 1, \Delta_\xi)|$ or $|(\Delta_S - 1, \Delta_\xi, \Delta_Q - 1)|$ respectively for $i = 1, 2, 3$ in the next part.

Second Part. We show that the function V from (7) admits a class $\mathcal{K}_\infty$ function $\sigma^\sharp$ such that

$$\dot{V}(t) \leq -\alpha(V(\tilde{S}(t), \tilde{\xi}(t), \tilde{Q}(t), \tilde{R}(t)) + \sigma^\sharp(|\epsilon^\sharp|_{[0,t]}) \tag{19}$$

along all solutions of the closed loop system from our Theorem 3.1 for all $t \geq 0$ when $|\epsilon|_\infty \leq \psi_*/4$, where α was defined in (8). This will provide the required ISS Lyapunov function decay condition in the variable $\tilde{x} = (\tilde{S}, \tilde{\xi}, \tilde{Q}, \tilde{R})$ that we will convert to the required ISS estimate in the original SIQR error variable $\tilde{X} = (S - S_*, I - I_*, Q - Q_*, R - R_*)$ at the end of the proof. By the decay estimate (9) on V from Lemma 2.1, (19) will be satisfied if we can find nonnegative valued nondecreasing functions σ_V, σ_I, and σ_C that are 0 at 0 such that

$$\begin{aligned}&-S(t)J_1(S(t), I(t))u_V(t) \leq \sigma_V(|\epsilon^\sharp|_{[0,t]}), \\ &-J_2(S(t), I(t), Q(t))u_I(t) \leq \sigma_I(|\epsilon^\sharp|_{[0,t]}), \text{ and} \\ &-J_3(S(t), I(t))u_C(t) \leq \sigma_C(|\epsilon^\sharp|_{[0,t]})\end{aligned}$$

along all trajectories of the closed loop system with initial states in $\mathcal{C}_0$ and disturbances $\epsilon^\sharp$ that are valued in $\mathcal{D}_0$ for all $t \geq 0$, which will let us pick $\sigma^\sharp = \sigma + \sigma_V + \sigma_I + \sigma_C$, where σ is from (8). Hence, we next construct σ_V, σ_I, and σ_C. To build σ_V, we consider two cases:

Case 1. Consider a $t \geq 0$ such that $-\hat{\rho} \geq \omega_V J_1(\Delta_S(t)S(t), \Delta_I(t)I(t))$. Then $J_1(\Delta_S(t)S(t), \Delta_I(t)I(t)) \leq 0$ (since $\omega_V > 0$ and $\hat{\rho} > 0$) and our formula for u_V from (12) gives $u_V(t) = -\hat{\rho}$, so (16) gives

$$\begin{aligned} -S(t)J_1(S(t), I(t))u_V(t) &= \hat{\rho}S(t)J_1(S(t), I(t)) \\ &\leq \hat{\rho}S(t)J_1(\Delta_S(t)S(t), \Delta_I(t)I(t)) \\ &\quad + \hat{\rho}S(t)\bar{J}_1|(\Delta_S(t) - 1, \Delta_\xi(t))| \\ &\leq \hat{\rho}\overline{\mathcal{C}}\bar{J}_1|(\Delta_S(t) - 1, \Delta_\xi(t))| \end{aligned}$$

Case 2. Consider a $t \geq 0$ such that $-\hat{\rho} < \omega_V J_1(\Delta_S(t)S(t), \Delta_I(t)I(t))$. Then the control value is $u_V(t) = \omega_V J_1(\Delta_S(t)S(t), \Delta_I(t)I(t))$, so

$$-S(t)J_1(S(t), I(t))u_V(t) = -\omega_V S(t)J_1(S(t), I(t))J_1(\Delta_S(t)S(t), \Delta_I(t)I(t)). \quad (20)$$

The right side of (20) is nonpositive if $\xi < -\xi_0$, by our choice of ξ_0. On the other hand, if we set

$$\bar{B}_V = \sup\{|J_1(S, I)| : \tilde{\xi} \geq -\xi_0, \tilde{\xi} = \ln(I/I_*), S \in (0, \overline{\mathcal{C}}], I \in (0, \overline{\mathcal{C}}]\},$$

then $\bar{B}_V < +\infty$. Therefore, in Case 2, if $\tilde{\xi}(t) \geq -\xi_0$, then we can use the bound (16) to get

$$\begin{aligned} -S(t)J_1(S(t), I(t))u_V(t) &\leq -\omega_V S(t)J_1^2(S(t), I(t)) \\ &\quad + \omega_V S(t)|J_1(S(t), I(t))|\bar{J}_1|(\Delta_S(t) - 1, \Delta_\xi(t))| \\ &\leq \omega_V \overline{\mathcal{C}}\bar{B}_V\bar{J}_1|(\Delta_S(t) - 1, \Delta_\xi(t))|. \end{aligned}$$

By combining the preceding two cases, we get

$$-S(t)J_1(S(t), I(t))u_V(t) \leq \overline{\mathcal{C}}\bar{J}_1 \max\{\hat{\rho}, \omega_V \bar{B}_V\}|(\Delta_S(t) - 1, \Delta_\xi(t))|$$

for all $t \geq 0$, so we can choose $\sigma_V(s) = \overline{\mathcal{C}}\bar{J}_1 \max\{\hat{\rho}, \omega_V \bar{B}_V\}s$. The same reasoning except without the $S(t)$ factors on the left sides of the preceding inequalities, and with J_1 replaced by J_2, and with the V subscripts replaced by I subscripts, and with $\hat{\rho}$ replaced by $\hat{\nu}$ and using (17) instead of (16), gives

$$-J_2(S(t), I(t), Q(t))u_I(t) \leq \bar{J}_2 \max\{\hat{\nu}, \omega_I \bar{B}_I\}|(\Delta_S(t) - 1, \Delta_\xi(t), \Delta_Q(t) - 1)|$$

for all $t \geq 0$, so we can choose $\sigma_I(s) = \bar{J}_2 \max\{\hat{\nu}, \omega_I \bar{B}_I\}s$. We next derive σ_C, by considering three cases.

Case 1. Consider a $t \geq 0$ where $J_3(\Delta_S(t)S(t), \Delta_I(t)I(t)) \geq 0$. Then our assumption on $\underline{\beta}$ and our formula for u_C from (12) gives $u_C(t) = 0$, so $-J_3(S(t), I(t))u_C(t) \leq 0$.

Case 2. Consider a $t \geq 0$ where $\omega_C J_3(\Delta_S(t)S(t), \Delta_I(t)I(t)) < \underline{\beta} - \hat{\beta}$. Then

$$u_C(t) = \underline{\beta} - \hat{\beta} \leq 0.$$

Also, by our choice of ξ_0, we have $\xi \geq -\xi_0$, since $\omega_C > 0$. Therefore, our bound (18) gives

$$\begin{aligned} -J_3(S(t), I(t))u_C(t) &= -J_3(S(t), I(t))(\underline{\beta} - \hat{\beta}) \\ &\leq -J_3(\Delta_S(t)S(t), \Delta_I(t)I(t))(\underline{\beta} - \hat{\beta}) \\ &\quad + \bar{J}_3(\hat{\beta} - \underline{\beta})|(\Delta_S - 1, \Delta_\xi)| \\ &\leq \bar{J}_3(\hat{\beta} - \underline{\beta})|(\Delta_S - 1, \Delta_\xi)|. \end{aligned}$$

Case 3. Consider a $t \geq 0$ where $\omega_C J_3(\Delta_S(t)S(t), \Delta_I(t)I(t)) \in [\underline{\beta} - \hat{\beta}, 0)$. Then (12) provides the control value $u_C(t) = \omega_C J_3(\Delta_S(t)S(t), \Delta_I(t)I(t))$, and our choice

$\xi_0 > 0$ again gives $\xi \geq -\xi_0$, so (18) gives

$$\begin{aligned} -J_3(S(t),I(t))u_C(t) &= -J_3(S(t),I(t))\omega_C J_3(\Delta_S(t)S(t),\Delta_I(t)I(t)) \\ &\leq -\omega_C J_3^2(S(t),I(t)) \\ &\quad +\omega_C|J_3(S(t),I(t))|\bar{J}_3|(\Delta_S(t)-1,\Delta_\xi(t))| \\ &\leq \omega_C\bar{B}_C\bar{J}_3|(\Delta_S(t)-1,\Delta_\xi(t))|, \end{aligned}$$

where $\bar{B}_C = \sup\{|J_3(S,I)| : \tilde{\xi} \geq -\xi_0, \tilde{\xi} = \ln(I/I_*), S \in (0,\overline{C}], I \in (0,\overline{C}]\}$. Combining the preceding cases lets us choose $\sigma_C(s) = \bar{J}_3 \max\{\hat{\beta} - \underline{\beta}, \omega_C\bar{B}_C\}s$.

Third Part. To obtain our exponential ISS condition (11), we first build positive constants $\overline{c}_i$ for $i = 1,2,3$ such that $\overline{c}_1|\tilde{x}|^2 \leq V(\tilde{x}) \leq \overline{c}_2|\tilde{x}|^2$ and $\alpha(V(\tilde{x})) \geq \overline{c}_3 V(\tilde{x})$ along all solutions of the closed loop system from the theorem. To this end, we first build positive constants $\underline{c}_i$ for $i = 1,2$ such that $\underline{c}_1|(\tilde{S},\tilde{\xi},\tilde{Q})|^2 \leq U(\tilde{S},\tilde{\xi},\tilde{Q}) \leq \underline{c}_2|(\tilde{S},\tilde{\xi},\tilde{Q})|^2$ along all solutions of this closed loop system, where U is the function defined in (7) that is used in the formula for V. To find $\underline{c}_1$, first note that we can find a constant $\underline{\xi} > 0$ such that

$$\begin{aligned} U(\tilde{S},\tilde{\xi},\tilde{Q}) &\geq \tfrac{c}{2}\left(\tfrac{\chi}{2\hat{\beta}}\right)^2\tilde{\xi}^2 \geq \tfrac{c}{4}\left(\tfrac{\chi}{2\hat{\beta}}\right)^2|(\tilde{S},\tilde{Q})|^2, \quad \text{hence} \\ U(\tilde{S},\tilde{\xi},\tilde{Q}) &\geq \tfrac{c}{4}\left(\tfrac{\chi}{2\hat{\beta}}\right)^2\tilde{\xi}^2 + \tfrac{c}{4}\left(\tfrac{\chi}{2\hat{\beta}}\right)^2\tilde{\xi}^2 \geq \tfrac{c}{4}\left(\tfrac{\chi}{2\hat{\beta}}\right)^2\tilde{\xi}^2 + \tfrac{c}{8}\left(\tfrac{\chi}{2\hat{\beta}}\right)^2|(\tilde{S},\tilde{Q})|^2 \\ &\geq \tfrac{c}{32}\left(\tfrac{\chi}{\hat{\beta}}\right)^2|(\tilde{S},\tilde{\xi},\tilde{Q})|^2 \end{aligned}$$

along all solutions of the closed loop system at all times when $\tilde{\xi} < -\underline{\xi}$, by the boundedness of $\mathcal{C}_1$. On the other hand, we can find a constant $c_a > 0$ such that

$$e^{\tilde{\xi}} - \tilde{\xi} - 1 \geq c_a\tilde{\xi}^2 \tag{21}$$

for all $\tilde{\xi} \geq -\underline{\xi}$, so (21) and our formula for U from (7) give

$$U(\tilde{S},\tilde{\xi},\tilde{Q}) \geq \tfrac{1}{2}\tilde{S}^2 + \tfrac{(c+1)\psi_* c_a}{\hat{\beta}}\tilde{\xi}^2 + \tfrac{c_\Diamond}{2}\tilde{Q}^2.$$

By separately considering the two cases where $\tilde{\xi} < -\underline{\xi}$ or $\tilde{\xi} \geq -\underline{\xi}$, it follows that we can pick

$$\underline{c}_1 = \min\left\{\tfrac{c\chi^2}{32\hat{\beta}^2}, \tfrac{1}{2}, \tfrac{c_\Diamond}{2}, \tfrac{(c+1)c_a\psi_*}{\hat{\beta}}\right\}.$$

To find $\underline{c}_2$, notice that we can find a constant $c_b > 0$ such that $\max\{(e^{\tilde{\xi}}-1)^2, |e^{\tilde{\xi}}-1-\tilde{\xi}|\} \leq c_b\tilde{\xi}^2$ along all solutions of the closed loop system (by separately considering cases where $\xi \leq -\xi_0$ and $\xi > -\xi_0$ for a big enough constant $\xi_0 > 0$, and by again using the boundedness of $\mathcal{C}_1$), so we can use the relation

$$\tfrac{c}{2}\left[\tilde{S} + \tfrac{\chi}{\hat{\beta}}\tilde{\xi} + I_*(e^{\tilde{\xi}} - 1)\right]^2 \leq \tfrac{3c}{2}\left[\tilde{S}^2 + \left(\tfrac{\chi}{\hat{\beta}}\right)^2\tilde{\xi}^2 + I_*^2 c_b\tilde{\xi}^2\right]$$

and our formula for U from (7) to conclude that we can satisfy our upper bounding condition on U using

$$\underline{c}_2 = \max\left\{\tfrac{1}{2}(1+3c), \tfrac{3c}{2}\left(\left(\tfrac{\chi}{\hat{\beta}}\right)^2 + I_*^2 c_b\right) + \tfrac{(c+1)\psi_*}{\hat{\beta}}c_b, \tfrac{1}{2}c_\Diamond\right\}.$$

Also, if $|\tilde{R}| \geq 2|\tilde{S} + I_*(e^{\tilde{\xi}} - 1) + \tilde{Q}|$, then the formula for W in our expression (7) for V satisfies $W(\tilde{S},\tilde{\xi},\tilde{Q},\tilde{R}) \geq \frac{g}{8}\tilde{R}^2$. If instead $|\tilde{R}| < 2|\tilde{S} + I_*(e^{\tilde{\xi}} - 1) + \tilde{Q}|$, then

$$\tilde{R}^2 \leq 6\big(\tilde{S}^2 + I_*^2(e^{\tilde{\xi}} - 1)^2 + \tilde{Q}^2\big) \leq 6\max\{1, I_*^2 c_b\}(\tilde{S}^2 + \tilde{\xi}^2 + \tilde{Q}^2),$$

and therefore also

$$\tfrac{\underline{c}_1}{12\max\{1,I_*^2c_b\}}\tilde{R}^2 \leq \tfrac{1}{2}\underline{c}_1(\tilde{S}^2+\tilde{\xi}^2+\tilde{Q}^2)$$

so we can use our lower bound $U(\tilde{S},\tilde{\xi},\tilde{Q}) \geq \underline{c}_1|(\tilde{S},\tilde{\xi},\tilde{Q})|^2$ to get

$$\begin{array}{l} V(\tilde{S},\tilde{\xi},\tilde{Q},\tilde{R}) \geq \tfrac{\underline{c}_1}{2}(\tilde{S}^2+\tilde{\xi}^2+\tilde{Q}^2)+\tfrac{\underline{c}_1}{2}(\tilde{S}^2+\tilde{\xi}^2+\tilde{Q}^2) \\ \geq \min\left\{\tfrac{\underline{c}_1}{2}, \tfrac{\underline{c}_1}{12\min\{1,I_*^2c_b\}}\right\}(\tilde{S}^2+\tilde{\xi}^2+\tilde{Q}^2+\tilde{R}^2). \end{array}$$

By separately considering the preceding two cases, we conclude that we can choose

$$\overline{c}_1 = \min\left\{\tfrac{\underline{c}_1}{2}, \tfrac{g}{8}, \tfrac{\underline{c}_1}{12\max\{1,I_*^2c_b\}}\right\}.$$

Also, since $W(\tilde{S},\tilde{\xi},\tilde{Q},\tilde{R}) \leq 2g(\tilde{S}^2+I_*^2(e^{\tilde{\xi}}-1)^2+\tilde{Q}^2+\tilde{R}^2)$, we can choose $\overline{c}_2 = \underline{c}_2 + 2g\max\{1,I_*^2c_b\}$.

To find $\overline{c}_3$, first note that we can use (19) to get

$$V(\tilde{x}(t)) \leq \max\{V(\tilde{x}(0)), \alpha^{-1}(2\sigma^\sharp(\overline{\epsilon}))\}$$

for all $t \geq 0$ for any bound $\overline{\epsilon} > 0$ on the elements of $\mathcal{D}_0$ when $|\epsilon|_\infty \leq \psi_*/4$, by separately considering the cases where $V(\tilde{x}(0)) \geq \alpha^{-1}(2\sigma^\sharp(\overline{\epsilon}))$ and $V(\tilde{x}(0)) < \alpha^{-1}(2\sigma^\sharp(\overline{\epsilon}))$ and using the fact that $\dot{V}(t) < 0$ when $\alpha(V(\tilde{x}(t))) \geq 2\sigma^\sharp(\overline{\epsilon})$. Hence, we can choose

$$\overline{c}_3 = \inf\{\alpha(s)/s : 0 < s \leq \max\{\overline{V}, \alpha^{-1}(2\sigma^\sharp(\overline{\epsilon}))\}\},$$

where $\overline{V} = \max\{V(p_1,p_2,p_3,p_4) : (p_1, I_*(e^{p_2}-1), p_3, p_4) \in \mathcal{C}_0\}$, which is defined because $\mathcal{C}_0$ is compact, and because we can use the formula for α from (8) and L'Hopital's rule to get $\lim_{s\to 0^+}(\alpha(s)/s) > 0$. Hence, by upper bounding $-\alpha(V(\tilde{x}(t))$ in (19) by $-\overline{c}_3V(\tilde{x}(t))$ and then applying an integrating factor to the result, we get

$$\begin{array}{l} \overline{c}_1|\tilde{x}(t)|^2 \leq V(\tilde{x}(t)) \leq e^{-\overline{c}_3t}V(\tilde{x}(0)) + \tfrac{1}{\overline{c}_3}\sigma^\sharp(|\epsilon^\sharp|_{[0,t]}) \\ \leq e^{-\overline{c}_3t}\overline{c}_2|\tilde{x}(0)|^2 + \tfrac{1}{\overline{c}_3}\sigma^\sharp(|\epsilon^\sharp|_{[0,t]}) \end{array} \tag{22}$$

and then we can divide (22) through by $\overline{c}_1$ and then use the subadditivity of the square root to get

$$|\tilde{x}(t)| \leq \sqrt{\tfrac{\overline{c}_2}{\overline{c}_1}}e^{-\overline{c}_3t/2}|\tilde{x}(0)| + \tfrac{1}{\sqrt{\overline{c}_1\overline{c}_3}}\sqrt{\sigma^\sharp(|\epsilon^\sharp|_{[0,t]})} \tag{23}$$

for all $t \geq 0$ along all of the solutions of the closed loop system when $|\epsilon|_\infty \leq \psi_*/4$. Also, we can find constants $\overline{d}_1 \in (0,1]$ and $\overline{d}_2 \geq 1$ such that $|\tilde{\xi}| \geq \overline{d}_1|\tilde{I}|$ at all times when $X = (S,I,Q,R)$ is in $\mathcal{C}_1$ and such that $|\tilde{\xi}| \leq \overline{d}_2|\tilde{I}|$ at all times when $\tilde{X} \in \mathcal{C}_0$, as follows. First, we can find a constant $\overline{\xi}_0 > 0$ such that $|\tilde{\xi}| \geq |\tilde{I}|$ when $\xi < -\overline{\xi}_0$; while for $\xi \geq -\overline{\xi}_0$ and at points where $X \in \mathcal{C}_1$, the Mean Value Theorem gives

$$|\tilde{I}| = |I - I_*| = |e^{\xi} - e^{\xi_*}| \leq e^{\max\{|\xi|,|\xi_*|\}}|\tilde{\xi}|.$$

Hence, we can choose

$$\overline{d}_1 = \min\{1, 1/\max\{e^{\max\{|\ln(I)|,|\xi_*|\}} : X \in \mathcal{C}_1, \xi \geq -\overline{\xi}_0\}\}.$$

To find $\overline{d}_2$, first write $|\tilde{\xi}| = |\ln(I) - \ln(I_*)| \leq L_*|\tilde{I}|$ for a Lipschitz constant $L_* \geq 1$ for ln on $\{I > 0 : \tilde{X} \in \mathcal{C}_0\}$, so we can take $\overline{d}_2 = L_*$. Therefore, if ϵ satisfies the additional requirement that $|\epsilon|_\infty \leq \psi_*/4$, then (23) gives

$$|\tilde{X}(t)| \leq \tfrac{\overline{d}_2}{\overline{d}_1}\sqrt{\tfrac{\overline{c}_2}{\overline{c}_1}}e^{-\overline{c}_3t/2}|\tilde{X}(0)| + \tfrac{1}{\overline{d}_1\sqrt{\overline{c}_1\overline{c}_3}}\sqrt{\sigma^\sharp(|\epsilon^\sharp|_{[0,t]})} \tag{24}$$

for all $t \geq 0$ along all solutions of the closed loop system from the theorem.

It remains to show how to eliminate the requirement that $|\epsilon|_\infty \leq \psi_*/4$. To this end, note that using the proof of [10, Theorem 3.2] except with $\Gamma(|\epsilon|_{[0,t]})$ replaced by the second term on the right side of (24), we get

$$|\tilde{X}(t)| \leq \overline{d}_3 e^{-\overline{c}_4 t}|\tilde{X}(0)| + \tfrac{1}{\overline{d}_1\sqrt{\overline{c}_1\overline{c}_3}}\sqrt{\sigma^\sharp(|\epsilon^\sharp|_{[0,t]})} + \overline{\Gamma}(|\epsilon|_{[0,t]}) \tag{25}$$

for all $t \geq 0$, where $\overline{c}_4 = \min\{\overline{c}_3/2, \mu\}$, $\overline{d}_3 = \max\{4, (\overline{d}_2/\overline{d}_1)\sqrt{\overline{c}_2/\overline{c}_1}\}$, and $\overline{\Gamma} \in \mathcal{K}_\infty$ is chosen such that

$$\overline{\Gamma}(s) \geq \tfrac{s+B}{\mu} + 5|(S_*, \xi_*, Q_*, R_*)| \text{ for all } s \geq \min\{B, \psi_*/4\},$$

and condition (25) is satisfied along all solutions of the SIQR error dynamics for $\tilde{X}$ satisfying the assumptions of the theorem, without requiring the additional condition that $|\epsilon|_\infty \leq \psi_*/4$. Choosing

$$\overline{\Gamma}(s) = \tfrac{s}{\mu} + \left(\tfrac{B}{\mu} + 5|(S_*, \xi_*, Q_*, R_*)|\right)\tfrac{s}{\min\{B, \psi_*/4\}},$$

then gives the required constants b_1, b_2, and r. □

Remark 3.2. A key ingredient in the proof of Theorem 3.1 is an equal sign condition, which called for a constant $\xi_0 > 0$ such that $J_1(\Delta_S S, \Delta_I I) < 0$, $J_1(S, I) < 0$, $J_2(\Delta_S S, \Delta_I I, \Delta_Q Q) < 0$, $J_2(S, I, Q) < 0$, $J_3(\Delta_S S, \Delta_I I) > 0$, and $J_3(S, I) > 0$ all hold for all $(S, I, Q, R) \in \mathcal{C}_1$ and all $(\Delta_S, \Delta_I, \Delta_Q)$ such that $\ln(I) = \xi < -\xi_0$ and such that $\epsilon^\sharp \in \mathcal{D}_0$, i.e., for each i, the J_i sign is equal at each state vector argument regardless of the uncertainty. This made it possible to prove semiglobal ISS estimates, namely, a collection of ISS estimates (11) that provide one ISS estimate for each pair $(\mathcal{C}_0, \mathcal{D}_0)$. In the next section, we provide an alternative ISS result, where the set of allowable values for the measurement uncertainties implies that the preceding equal signs conclusions are satisfied without requiring that the ξ take sufficiently negative values.

4. **Robust ISS result.** Theorem 3.1 provides $\Phi \in \mathcal{KL}$ and $\Gamma \in \mathcal{K}_\infty$ such that all solutions $\tilde{X}(t) = (\tilde{S}(t), \tilde{I}(t), \tilde{Q}(t), \tilde{R}(t))$ of the SIQR error dynamics with initial states in $\mathcal{C}_0$ for all disturbances satisfying the assumptions of the theorem satisfy

$$|(\tilde{S}(t), \tilde{I}(t), \tilde{Q}(r), \tilde{R}(t))| \leq \Phi(|(\tilde{S}(0), \tilde{I}(0), \tilde{Q}(0), \tilde{R}(0))|, t) + \Gamma(|\epsilon^\sharp|_{[0,t]})$$

for all $t \geq 0$, where Φ and Γ depend on $\mathcal{C}_0$ and on the set of admissible values $\mathcal{D}_0$ for the disturbance functions. Hence, the solutions of the closed loop system converge to 0 (so the states of the original SIQR dynamics (1) converge to the endemic equilibrium) as $t \to +\infty$ with an overshoot $\Gamma(|\epsilon^\sharp|_{[0,t]})$ depending on the immigration disturbance ϵ and the multiplicative disturbance functions Δ_S, Δ_I, and Δ_Q.

Under alternative conditions, we can prove an analog where the overshoot only depends on the immigration uncertainty ϵ instead of $\epsilon^\sharp$. To state this analog, we fix any constant $c > 0$, and we use the functions

$$\begin{aligned}
\mathcal{M}_1(S, I, d_1, d_2) &= (c+1)(d_1 - 1)S + c\left[\tfrac{\hat{\rho}+\mu}{\hat{\beta}}d_2 + (e^{d_2} - 1)I\right], \\
\mathcal{M}_2(S, I, Q, d_1, d_2, d_3) &= c\left((d_1 - 1)S + \tfrac{\hat{\rho}+\mu}{\hat{\beta}}d_2 + (e^{d_2} - 1)I\right)\left(\tfrac{\hat{\rho}+\mu}{\hat{\beta}} + e^{d_2}I\right) \\
&\quad + c\left(S - S_* + \tfrac{\hat{\rho}+\mu}{\hat{\beta}}\ln\left(\tfrac{I}{I_*}\right) + I - I_*\right)(e^{d_2} - 1)I \\
&\quad + \tfrac{(c+1)(\gamma+\hat{\nu}+\mu)}{\hat{\beta}}(e^{d_2} - 1)I - (e^{d_2} - 1)Ic_\diamondsuit(d_3 Q - Q_*) \\
&\quad - Ic_\diamondsuit(d_3 - 1)Q, \text{ and}
\end{aligned} \tag{26}$$

$$\begin{aligned}\mathcal{M}_3(S,I,d_1,d_2) &= (d_1-1)S\Big[(d_1S-S_*)e^{d_2}I - c\Big\{d_1S-S_*\\ &\quad +\tfrac{\hat\rho+\mu}{\hat\beta}\left[\ln\left(\tfrac{I}{I_*}\right)+d_2\right]+e^{d_2}I-I_*\Big\}\tfrac{\hat\rho+\mu}{\hat\beta}\\ &\quad -\tfrac{(c+1)(\gamma+\hat\nu+\mu)}{\hat\beta}(e^{d_2}I-I_*)\Big]+S\Big[(d_1-1)Se^{d_2}I\\ &\quad +\tilde S(e^{d_2}-1)I\\ &\quad -c\left((d_1-1)S+\tfrac{\hat\rho+\mu}{\hat\beta}d_2+(e^{d_2}-1)I\right)\tfrac{\hat\rho+\mu}{\hat\beta}\\ &\quad -\tfrac{(c+1)(\gamma+\hat\nu+\mu)}{\hat\beta}(e^{d_2}-1)I\Big]\end{aligned} \tag{27}$$

with the notation from above. The motivation for the preceding functions is that (13)-(14) give

$$\begin{aligned}&J_i(\Delta_S S,\Delta_I I)=J_i(S,I)+\mathcal{M}_i(S,I,\Delta_S,\Delta_\xi) \text{ for } i=1,3 \text{ and}\\ &J_2(\Delta_S S,\Delta_I I,\Delta_Q Q)=J_2(S,I,Q)+\mathcal{M}_2(S,I,Q,\Delta_S,\Delta_\xi,\Delta_Q)\end{aligned}$$

for all state and disturbance values. Therefore, for $i=1$ and $i=3$, $J_i(\Delta_S S,\Delta_I I)$ and $J_i(S,I)$ have the same sign if and only if $|\mathcal{M}_i(S,I,\Delta_S,\Delta_\xi)| \leq |J_i(S,I)|$, and also, $J_2(\Delta_S S,\Delta_I I,\Delta_Q Q)$ and $J_2(S,I,Q)$ have the same sign if and only if $|\mathcal{M}_2(S,I,Q,\Delta_S,\Delta_\xi,\Delta_Q)| \leq |J_2(S,I,Q)|$. This motivates our choice of the set

$$\begin{aligned}&\mathcal{D}_{\mathcal{M}}(S,I,Q)=\\ &\big\{(d_1,d_2,d_3): |\mathcal{M}_i(S,I,d_1,d_2)| \leq |J_i(S,I)| \text{ for } i=1 \text{ and } 3,\\ &|\mathcal{M}_2(S,I,Q,d_1,d_2,d_3)| \leq |J_2(S,I,Q)|\big\},\end{aligned} \tag{28}$$

and the following theorem:

Theorem 4.1. *For each set of positive constants $\hat\rho$, $\hat\nu$, $\hat\beta$, c, ω_V, ω_I, and ω_C, and each constant $\underline{\beta} \in [0,\hat\beta)$, there exist functions $\Phi \in \mathcal{KL}$ and $\Gamma \in \mathcal{K}_\infty$ depending on the preceding constants such that for all solutions $(\tilde S(t),\tilde I(t),\tilde Q(t),\tilde R(t))$ of the SIQR error dynamics in closed loop with the controls (10) and all piecewise continuous locally bounded choices of $\epsilon:[0,+\infty)\to(-B,+\infty)$ such that $|\epsilon|_\infty \leq \psi_*/4$ and all piecewise continuous locally bounded choices of $(\Delta_S,\Delta_I,\Delta_Q):[0,+\infty)\to(0,+\infty)^3$ that satisfy $(\Delta_S(t),\ln(\Delta_I(t)),\Delta_Q(t)) \in \mathcal{D}_{\mathcal{M}}(S(t),I(t),Q(t))$ for all $t\geq 0$, the following bound is satisfied:*

$$|(\tilde S(t),\tilde I(t),\tilde Q(t),\tilde R(t))| \leq \Phi(|(\tilde S(0),\tilde I(0),\tilde Q(0),\tilde R(0))|,t)+\Gamma(|\epsilon|_{[0,t]}). \tag{29}$$

for all $t\geq 0$.

Proof. We again use the strict Lyapunov function V from (7). Along all solutions of the closed loop system, Lemma 2.1 provides class $\mathcal{K}_\infty$ functions α and σ_0 such that

$$\begin{aligned}\dot V(t) \leq\ & -\alpha(V(\tilde S(t),\tilde\xi(t),\tilde Q(t),\tilde R(t)) - \{S(t)J_1(S(t),I(t))u_V(t)\\ &+J_2(S(t),I(t),Q(t))u_I(t)+J_3(S(t),I(t))u_C(t)\}+\sigma_0(|\epsilon|_{[0,t]})\end{aligned} \tag{30}$$

holds for all $t\geq 0$ along all solutions of the closed loop system. Therefore, by considering the cases that we studied in the second part of the proof of Theorem 3.1, it suffices to show that the quantity in curly braces in (30) is nonnegative. By reasoning that is similar to the second part of the proof of Theorem 3.1, this nonnegativity will hold if

$$\text{sgn}(J_1(S(t),I(t))) = \text{sgn}(J_1(\Delta_S(t)S(t),\Delta_I(t)I(t)))$$

and

$$\operatorname{sgn}(J_2(S(t),I(t),Q(t))) = \operatorname{sgn}(J_2(\Delta_S(t)S(t),\Delta_I(t)I(t),\Delta_Q(t)Q(t)))$$

and

$$\operatorname{sgn}(J_3(S(t),I(t))) = \operatorname{sgn}(J_3(\Delta_S(t)S(t),\Delta_I(t)I(t)))$$

hold along all solutions of the closed loop system. As explained above, this equal signs condition is equivalent to the requirements that $|\mathcal{M}_i(S,I,\Delta_S,\Delta_\xi)| \leq |J_i(S,I)|$, for $i=1$ and $i=3$ and that $|\mathcal{M}_2(S,I,Q,\Delta_S,\Delta_\xi,\Delta_Q)| \leq |J_2(S,I,Q)|$. This in turn is equivalent to the inequalities in the definition of $\mathcal{D}_{\mathcal{M}}(S,I,Q)$ holding at all times $t \geq 0$ with the choices $(d_1,d_2,d_3) = (\Delta_S, \ln(\Delta_I), \Delta_Q)$. The theorem now follows from our assumption that $(\Delta_S(t), \ln(\Delta_I(t)), \Delta_Q(t)) \in \mathcal{D}_{\mathcal{M}}(S(t),I(t),Q(t))$ for all $t \geq 0$. □

Remark 4.2. Theorem 4.1 includes a robust global asymptotic stability result, namely, when $\epsilon(t)$ is the zero function, then the overshoot $\Gamma(|\epsilon|_{[0,t]})$ in the final ISS estimate (29) is zero so (29) is a global asymptotic stability estimate for all choices of the other uncertainty functions $\Delta_S(t)$, $\Delta_I(t)$, and $\Delta_Q(t)$ that satisfy the assumptions of the theorem. This differs from traditional robust asymptotic stability results, where the bounds on the uncertainty ensuring asymptotic stability are constant, because here, the set $\mathcal{D}_{\mathcal{M}}(S(t),I(t),Q(t))$ that must contain $(\Delta_S(t),\Delta_\xi(t),\Delta_Q(t))$ at each time t is a time-varying set instead of a fixed compact box.

Hence, key differences between Theorems 3.1 and 4.1 above are that (a) Theorem 4.1 eliminates the effects of Δ_S, Δ_I, and Δ_Q from the added overshoot term in the final ISS estimate, (b) whereas the conclusion of Theorem 3.1 is semi-global insofar that its constants b_1, b_2, and r depend on the compact sets $\mathcal{C}_0$ and $\mathcal{D}_0$, the conclusion of Theorem 4.1 is a global one that produces comparison functions Φ and Γ that are independent of the sets of initial states, (c) the conclusion of Theorem 4.1 is not an exponential stability one like it is in the conclusion of Theorem 3.1, and (d) Theorem 4.1 adds the condition $|\epsilon|_\infty \leq \psi_*/4$ that was not present in the conclusion of Theorem 3.1 but which was needed in [10, Theorem 1]. On the other hand, if we add the assumption to Theorem 4.1 that there is a compact subset $\mathcal{D}_0 \subseteq (-B,+\infty)\times(-\infty,1)\times\mathbb{R}\times(-\infty,1)$ such that $(\epsilon(t), 1-\Delta_S(t), \ln(\Delta_I(t)), 1-\Delta_Q(t)) \in \mathcal{D}_0$ for all $t \geq 0$, and if we only consider solutions of the SIQR dynamics whose initial states lies in in a given compact set $\mathcal{C}_0$ of initial states, then the proof of Theorem 4.1 and the third part of the proof of Theorem 3.1 provide positive constants b_1, b_2, and r such that

$$\begin{aligned}|(\tilde{S}(t),\tilde{I}(t),\tilde{Q}(t),\tilde{R}(t))| \;\leq\; & b_1|(\tilde{S}(0),\tilde{I}(0),\tilde{Q}(0),\tilde{R}(0))|e^{-rt} \\ & + b_2\left(|\epsilon|_{[0,t]} + \sqrt{|\epsilon|_{[0,t]}+|\epsilon|^2_{[0,t]}}\right)\end{aligned}$$

for all $t \geq 0$ along all solutions of the closed loop system from Theorem 4.1 with initial states in $\mathcal{C}_0$ whose uncertainties satisfy the additional requirement that $(\epsilon(t), 1-\Delta_S(t), \ln(\Delta_I(t)), 1-\Delta_Q(t)) \in \mathcal{D}_0$ for all $t \geq 0$, where b_1, b_2, and r again depend on $\mathcal{C}_0$ and $\mathcal{D}_0$, but where the condition $|\epsilon|_\infty \leq \psi_*/4$ is no longer required.

Remark 4.3. Our uncertainties Δ_S, Δ_I, and Δ_Q can model the effects of sampling or time delays in the measurements of S, I, and Q, e.g., lags between the times that perturbed population measurements are taken and the times that the feedback controls can be implemented. For instance, consider the case where the available S measurement at each $t \geq 0$ is $\Delta_S^*(t)S(t-d_S(t))$ where Δ_S^* is a piecewise continuous

unknown function that represents measurement uncertainty as before and $d_S(t)$ denotes a time delay. This models the effects of sampled measurements at sample times $\{t_i\}$ that admit constants $\underline{t} > 0$ and $\overline{t} > 0$ such that $t_0 = 0$ and $t_{i+1} - t_i \in [\underline{t}, \overline{t}]$ for $i = 0, 1, 2, \ldots$, by choosing $d_S(t) = t - \Sigma(t)$ for all $t \geq 0$, where $\Sigma(t)$ is the largest sample time on each interval $[0, t]$ for each $t \geq 0$. This produces sawtooth-shaped discontinuous delays d_S. Then we can choose $\Delta_S(t) = \Delta_S^*(t)S(t - d_S(t))/S(t)$ for all $t \geq 0$ to get $\Delta_S(t)S(t) = \Delta_S^*(t)S(t - d_S(t))$ for all $t \geq 0$, and similar reasoning applies to I and Q. This is an analog of the delayed results from [10, Section 5], which analyzed the effects of delayed measurements in the unperturbed controls (3) but did not allow the multiplicative measurement uncertainties in the measurements in the feedback controls that we allow here.

Remark 4.4. Since Theorems 3.1-4.1 assume that the constants $\hat{\rho}$ and ω_V in the control formulas in (2) and (10) are positive, the statements of these theorems do not allow cases where no vaccination control is present. However, the conclusions of the two theorems remain true if we change their assumptions by instead having $\hat{\rho} = \omega_V = 0$ and keep all other assumptions the same, and this covers cases where no vaccination is being used. Their proofs remain the same with this change, except the σ_V in the proof of Theorem 3.1 is the zero function. We illustrate this variant of the theorems in the next section.

5. Simulations and discussions.

5.1. **Objectives.** We present our `MATLAB` simulations to illustrate the effectiveness of the feedback controls (10). In [10], the values for the constants in the model and in the controls were chosen to model the COVID-19 pandemic in Japan, and we use the same parameter settings in this section; see Table 1 for parameter descriptions, settings, and the sources of those parameter values. The unit of population is in millions, and the time t is in days. As in [10], we assume a 20% perturbation of immigrants and newborns, which gives

$$\epsilon(t) = -311 \times 10^{-6} \cos(\pi t/150) \tag{31}$$

and the computed basic reproduction number $\hat{R}_0$ from (2) is 1.1001 when vaccination is being used.

For our simulations, we study how the feedback controls and states change due to the measurement uncertainties Δ_S, Δ_I, and Δ_Q in (10) and we consider the biological implications of these results. We first study cases of constant uncertainties that correspond to undercounting or overcounting. The majority of the experiments focus on undercounting. To curtail the spread of disease, underestimating the number of infectious individuals can be a more serious problem than overestimating. Undercounting the infected compartments can be expected due to reluctance of individuals to be tested, insufficiently many test kits, false negative test results, and a significant number of untested asymptomatic infected individuals. We also consider mixed constant levels of uncertainty occur due to undercounting in classes I and Q and overcounting in S because undercounting of I and Q could result in an overcounting of the susceptible population. We also consider what happens with these constant levels of uncertainties in the absence of vaccination, as described in Remark 4.4. This simulates cases of the beginning stages of an outbreak of a novel strain (like COVID or the 2009 swine flu pandemic) when a vaccine is being developed but not yet readily available.

We also study cases where Δ_S, Δ_I, and Δ_Q vary over time. These uncertainties account for undercounting. The uncertainties that we consider are sigmoidal Hill functions (with varying heights) and periodic (for varying periods). The Hill functions model increases in resources (e.g., test kits, vaccines, and resources needed to administer such products) that can improve measurements over time. The periodic functions model population participation in vaccination and testing fluctuating over time. Lastly, we study how the feedback controls and states change due to time-varying uncertainties that are generated from Theorem 4.1.

5.2. **Description of numerical implementation.** For numerical simulations to illustrate Theorem 3.1 in which Δ_S , Δ_I, and Δ_Q are specified, we generate solutions for states and controls using an iterative process involving the Runge-Kutta method. With specified controls and uncertainty functions, the system is of the form $\dot{x}(t) = f(t, x(t))$, for which `MATLAB`'s ODE solvers (like `ode23` and `ode45`) can generate solutions for any initial conditions. However, we build a numerical scheme that can be modified to handle the constraints in Theorem 4.1 and is similar in spirit to the forward-backward sweep method (e.g., from [17, Chapter 4]), which is commonly used in mathematical biology.

Our numerical scheme is as follows. First, we partition the time interval $[0, T]$ into $n+1$ equally spaced nodes, with mesh size $h = T/n$. For the simulations where the uncertainty measures are specified, we set T equal to 500 days and n set to being 5000, so the mesh size is $h = 0.1$. We denote the kth mesh point kh by t_k for each k. We construct an $n+1$ vector for each state variable S, I, Q, and R, which are denoted by $\boldsymbol{S}$, $\boldsymbol{I}$, $\boldsymbol{Q}$, and $\boldsymbol{R}$ respectively, and an $n+1$ vector for each control variable u_i for $i = C, I, V$ which are denoted by $\boldsymbol{u}_i$ respectively, whose entries are the value of the variables at the mesh points, so for instance, the kth entry of $\boldsymbol{S}$ is $S_k = S(t_k)$ and the kth entry of $\boldsymbol{u}_V$ is denoted by $u_{V,k} = u_V(t_k)$ for $k = 0, \ldots, n$. The values of these $n+1$ vectors are updated in an iterative procedure that we explain below. We use superscripts to indicate these updated values, as follows. For $i = C, I, V$, $\boldsymbol{u}_i^j$ is the jth update of $\boldsymbol{u}_i$ for all $j \geq 0$, where the 0th update is initialized as described in Step 1. Similarly, $\boldsymbol{S}^j$, $\boldsymbol{I}^j$, $\boldsymbol{Q}^j$, and $\boldsymbol{R}^j$ are the jth updates of these vectors, but the first entry of each vector is set based on the initial values. Additionally, for $\ell = S, I$, and Q we construct an $n+1$ vector for each input Δ_ℓ, which is denoted $\boldsymbol{\Delta_\ell}$ whose kth entry is defined as $\boldsymbol{\Delta}_{\ell,k} = \Delta_\ell(t_k)$. These vectors are fixed during this iterative process. In the descriptions below, we use the definition $\boldsymbol{X}^j = (\boldsymbol{S}^j, \boldsymbol{I}^j, \boldsymbol{Q}^j, \boldsymbol{R}^j)$ which is an $(n+1)\times 4$ matrix whose columns $\boldsymbol{X}^j_{*,\ell}$ correspond to the jth iteration of state vector $\boldsymbol{\ell}^j$ for $\ell = S, I, Q$, and R. The numerical scheme is as follows:

Step 1. Initialize $\boldsymbol{u}_i^0$ to be the zero vector for all i. For initializing $\boldsymbol{X}^0$, let $\boldsymbol{X}^0_0 = (S(0), I(0), Q(0), R(0)) = (S_0, I_0, Q_0, R_0)$ given in Table 1. Fix vectors $\boldsymbol{\Delta_\ell}$ and the convergence tolerance parameter δ.

Step 2. To obtain the iterates $\boldsymbol{X}^{j+1}$ for $j \geq 0$, we treat (1) as an initial value problem with the initial state $(S(0), I(0), Q(0), R(0)) = (S_0, I_0, Q_0, R_0)$ in Table 1 and the immigration uncertainty in (31). set $\boldsymbol{X}^j_0 = \boldsymbol{X}^0_0$ for all j. We use a fourth-order Runge-Kutta routine to numerically solve (1) forward in time, with the control being the previous iteration of the controls $\boldsymbol{u}_i^j$.

Step 3. After generating $\boldsymbol{X}^{j+1}$, we use (10) with the values of the measurement uncertainties that we specify below to compute the feedback control values, which we denote as $\tilde{\boldsymbol{u}}_i^j$, and set $\boldsymbol{u}_i^{j+1} = 0.5\boldsymbol{u}_i^j + 0.5\tilde{\boldsymbol{u}}_i^j$.

Step 4. We check for convergence. We measure the relative error between the current and previous iterate of the states and between the current and previous iterate of the controls. Let $\|\cdot\|$ be the Euclidean 1-norm, i.e., $\|\mathbf{y}\| = |y_1| + \ldots |y_n|$. If both $\delta\|\boldsymbol{u}_i^j\| - \|\boldsymbol{u}_i^{j+1} - \boldsymbol{u}_i^j\| \geq 0$ for all $i = C, I, V$ and $\delta\|\boldsymbol{X}_{*,\ell}^{j+1}\| - \|\boldsymbol{X}_{*,\ell}^{j+1} - \boldsymbol{X}_{*,\ell}^{j}\| \geq 0$ for all $\ell = S, I, Q$, and R, then output their current values as solutions; otherwise, if any of these values violate the above inequalities, then return to Step 2.

For Step 3, we use a convex combination to update the controls to speed up convergence, and we use $\delta = 10^{-8}$. The main differences between our technique and the forward-backward sweep are that there is no backward implementation of Runge-Kutta (since our method has no costate variables to update) and the control is a feedback (instead of an optimal) control. See Fig. 1 for a flow chart explaining our method.

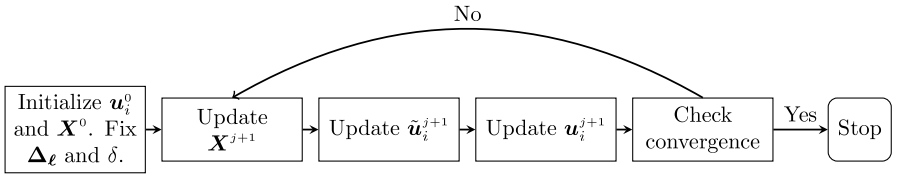

FIGURE 1. Flow chart when Δ_S, Δ_I, and Δ_Q are specified.

To construct uncertainty measurements for which the overshoot function depends only on the immigration disturbance function ϵ, we apply Theorem 4.1. For our experiments, due to our settings for immigration disturbances that satisfy $|\epsilon|_\infty > \psi_*/4$, we are simulating results corresponding to Remark 4.2. To find uncertainty values that satisfy the requirements $(d_1(t), d_2(t), d_3(t)) = (\Delta_S(t), \ln(\Delta_I(t)), \Delta_Q(t)) \in \mathcal{D}_{\mathcal{M}}(S(t), I(t), Q(t))$ for all $t \geq 0$ from Theorem 4.1, we can consider the following optimization problem:

$$\begin{array}{ll} \min\limits_{d_1,d_2,d_3} & J(d_1(t), d_2(t), d_3(t)) = 0 \\ \text{subject to} & |\mathcal{M}_1(S(t), I(t), d_1(t), d_2(t))| - |J_1(S(t), I(t))| \leq 0 \\ & |\mathcal{M}_2(S(t), I(t), Q(t), d_1(t), d_2(t), d_3(t))| - |J_2(S(t), I(t), Q(t))| \leq 0 \\ & |\mathcal{M}_3(S(t), I(t), d_1(t), d_2(t))| - |J_3(S(t), I(t))| \leq 0 \\ & 0 < d_1(t) \leq 1, d_2(t) \leq 0, \ 0 < d_3(t) \leq 1 \\ & \text{for all } t \geq 0, \end{array} \tag{32}$$

where $\mathcal{M}_i$ and J_i are defined above (in the first part of the proof of Theorem 3.1 and (26)-(27)) and the immigration perturbation as defined in (31) is also applied in the above problem. Our methods cover more general cases where the constraints in the last line are only that $0 < d_1(t)$ and $0 < d_3(t)$ for all $t \geq 0$; however, in our experiments we restricted the problem to where we are searching for uncertainty measures that correspond to undercounting in classes S, I, and Q. Since $d_2(t) = \ln(\Delta_I(t))$, the inequality constraint $d_2(t) \leq 0$ corresponds to the constraint $0 < \Delta_I(t) \leq 1$. The objective function used in (32) is set to 0 to simply find a solution that satisfies the inequality constraints, but other objective functions can be used.

For computational purposes, we performed our simulations by solving a discretized variant of (32) over time interval $[0, T]$, with $T = 250$. We partition the time interval as described in our previous simulations with the same mesh size being considered. We construct an $n+1$ vector of d_m for $m = 1, 2, 3$, and we use bold font for these symbols to express these vectors. For $m = 1, 2, 3$, the kth entry of $\boldsymbol{d}_m$ is

defined by $d_{m,k} = d_m(t_k)$ for $k = 0, \ldots, n$. The discretized variant of problem (32) is:

$$\begin{array}{ll} \min\limits_{(\boldsymbol{d_1},\boldsymbol{d_2},\boldsymbol{d_3})} & J(\boldsymbol{d}_1, \boldsymbol{d}_2, \boldsymbol{d}_3) = 0 \\ \text{subject to} & |\mathcal{M}_1(S_k, I_k, d_{1,k}, d_{2,k})| - |J_1(S_k, I_k)| \leq 0 \\ & |\mathcal{M}_2(S_k, I_k, Q_k, d_{1,k}, d_{2,k}, d_{3,k})| - |J_2(S_k, I_k, Q_k)| \leq 0 \\ & |\mathcal{M}_3(S_k, I_k, d_{1,k}, d_{2,k})| - |J_3(S_k, I_k)| \leq 0 \\ & \text{for all } k = 0, \ldots, n, \\ & \mathbf{0} < \boldsymbol{d_1} \leq \mathbf{1}, \mathbf{0} < \boldsymbol{d}_3 \leq \mathbf{1}, \text{ and } \boldsymbol{d_2} \leq \mathbf{0}, \end{array} \tag{33}$$

where $\mathbf{0} \in \mathbb{R}^{n+1}$ is the vector of all zeros and $\mathbf{1} \in \mathbb{R}^{n+1}$ is the vector of all 1's, and the inequalities in the last line of (33) should be understood to hold componentwise.

In numerically solving problem (33), we use `MATLAB`'s optimization solver `fmincon` which handles large scale nonlinear constrained optimization problems using an iterative procedure called the interior-point method. In using `fmincon`, we rewrote each nonlinear constraint $|\mathcal{M}_i(\cdot)| - |J_i(\cdot)| \leq 0$ as the two inequality constraints $\mathcal{M}_i(\cdot) - |J_i(\cdot)| \leq 0$ and $-\mathcal{M}_i(\cdot) - |J_i(\cdot)| \leq 0$ so that the function generated by the left hand side of each of these inequalities is differentiable with respect to $d_{m,k}$. We solve (33) to produce a sequence of triplets $(\boldsymbol{d_1^j}, \boldsymbol{d_2^j}, \boldsymbol{d_3^j})$ for the jth iterate in the algorithm that we state next. When using `fmincon`, we chose initial values $\boldsymbol{d}_m^0$ for $m = 1, 2, 3$ to be randomly generated values corresponding to overcounting rather than undercounting because with such initialization the solver ran faster and the final update satisfied all of the constraints given in problem (32). In numerically implementing simulations corresponding to Theorem 4.1 and Remark 4.2, we perform the following, where we continue our other notation for state and control sequences:

Step 1. Initialize each control $\boldsymbol{u}_i^0$ as being the all zeros vector. In order to initialize $\boldsymbol{X}^0$, let $\boldsymbol{X}_0^0 = (S(0), I(0), Q(0), R(0)) = (S_0, I_0, Q_0, R_0)$ given in Table 1. Initialize the uncertainty measures as $\boldsymbol{d}_1^0 = \mathbf{1} + \texttt{rand}(1, n+1)$, $\boldsymbol{d}_3^0 = \mathbf{1} + \texttt{rand}(1, n+1)$, and $\boldsymbol{d}_2^0 = \texttt{rand}(1, n+1)$, where $\texttt{rand}(1, n+1)$ is a `MATLAB` command that generates an $n+1$ vector whose entries are randomly generated numbers on $(0, 1]$. Fix the convergence tolerance parameter δ.

Step 2. Using the initial values $(S(0), I(0), Q(0), R(0)) = (S_0, I_0, Q_0, R_0)$ from Table 1 and the values of the previous iteration $\boldsymbol{u}^j$ of the controls for $j \geq 0$, apply a fourth-order Runge-Kutta routine to simultaneously update all of the states $\boldsymbol{X}^{j+1}$ forward in time according to the system of equations in (1).

Step 3. Use `fmincon` to solve (33) with the S_k, I_k, Q_k, and R_k values chosen to be the corresponding components of the newly updated states $\boldsymbol{X}^{j+1}$. For updating $\boldsymbol{d}_m^{j+1}$, we use a convex combination of the previous iterate $\boldsymbol{d}_m^j$ and the numerical solution $\boldsymbol{d}_m^{j+1*}$ to (33). That is, $\boldsymbol{d}_m^{j+1} = 0.5\boldsymbol{d}_m^j + 0.5\boldsymbol{d}_m^{j+1*}$.

Step 4. After generating the updated states $\boldsymbol{X}^{j+1}$ and uncertainty measures $\boldsymbol{d}_m^{j+1}$, use (10) to compute the feedback controls, which we denote as $\tilde{\boldsymbol{u}}_i^j$, and set $\boldsymbol{u}_i^{j+1} = 0.5\boldsymbol{u}_i^j + 0.5\tilde{\boldsymbol{u}}_i^j$.

Step 5. We check for convergence. Here we wish to measure the relative error between the current and previous iterate of the states and between the current and previous iterate of the controls. Let $\|\cdot\|$ denote the Euclidean 1-norm as before. If both $\delta\|\boldsymbol{u}_i^j\| - \|\boldsymbol{u}_i^{j+1} - \boldsymbol{u}_i^j\| \geq 0$ for $i = C, I, V$ and $\delta\|\boldsymbol{X}_{*,\ell}^{j+1}\| - \|\boldsymbol{X}_{*,\ell}^{j+1} - \boldsymbol{X}_{*,\ell}^j\| \geq 0$ for all $\ell = S, I, Q$, and R, then output their current values as solutions; otherwise, if any of these values violate the above inequalities, then return to Step 2. See Fig. 2 for a flow chart describing these steps.

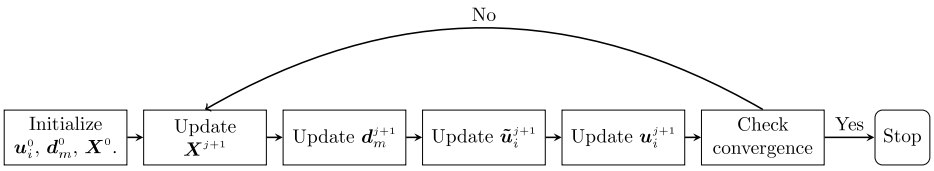

FIGURE 2. Flow chart for applying Theorem 4.1.

For using `fmincon`, we had to adjust the "MaximumFunctionEvaluations" to being 500,000 (although we can decrease this setting if we were to run this problem over a smaller time interval). Additionally, in using `fmincon` to solve the discretized problem, we had to set our model parameters and state variables as being global variables. A convex combination between the previous control values and the values generated by the feedback control is used in Step 4 for speeding up convergence. For our simulations pertaining to Theorem 4.1, we used $\delta = 10^{-6}$, and we generate solutions over the time interval $[0, 250]$.

5.3. **Constant levels of uncertainty.** We first study constant levels of uncertainty measures in compartments S, I, and Q to investigate how such measures (and the immigration perturbation (31)) influence the behaviors of the controls and the states. These uncertainty measurements correspond to uncertainties due to undercounting or overcounting. The percentage of undercounting class ℓ is obtained by computing $1 - \Delta_\ell$ (for $\ell = S,\ I$, and Q), and the percentage of overcounting class ℓ is obtained by computing $\Delta_\ell - 1$ (for $\ell = S,\ I$, and Q). For our simulations, we compare our results to the case in which no measurement uncertainties are being applied to the classes ($\Delta_\ell = 1$ for all $\ell = S,\ I$, and Q). In all of these simulations, we have the immigration perturbation set as (31). We conducted these types of simulations associated with constant levels of uncertainty:

1. Measurement uncertainties applied to classes S, I, and Q that correspond to undercounting each class for varying percentage levels of undercounting, using the parameter values from Table 1. The percentage levels are 20% undercounting of each class ($\Delta_\ell = 0.8$ for $\ell = S,\ I,\ Q$), 30% undercounting of each class ($\Delta_\ell = 0.7$ for $\ell = S,\ I,\ Q$), 50% undercounting of each class ($\Delta_\ell = 0.5$ for $\ell = S,\ I,\ Q$), 70% undercounting ($\Delta_\ell = 0.3$ for $\ell = S,\ I,\ Q$), and 80% undercounting ($\Delta_\ell = 0.2$ for $\ell = S,\ I,\ Q$).
2. Measurement uncertainties applied to classes S, I, and Q that correspond to undercounting each class for varying percentage levels of undercounting in the absence of vaccination (as in Remark 4.4), which correspond to choosing $\hat{\rho} = \omega_V = 0$ in the simulations. The percentage levels are 20% undercounting of each class ($\Delta_\ell = 0.8$ for $\ell = S,\ I,\ Q$), 30% undercounting of each class ($\Delta_\ell = 0.7$ for $\ell = S,\ I,\ Q$), 50% undercounting of each class ($\Delta_\ell = 0.5$ for $\ell = S,\ I,\ Q$), 70% undercounting ($\Delta_\ell = 0.3$ for $\ell = S,\ I,\ Q$), and 80% undercounting ($\Delta_\ell = 0.2$ for $\ell = S,\ I,\ Q$).
3. Measurement uncertainties applied to S, I, and Q that correspond to undercounting class I and Q and overcounting class S for varying percentage levels using the values from Table 1. The percentage levels are 20% undercounting in class I and Q ($\Delta_\ell = 0.8$ for $\ell = I, Q$) and 20% overcounting in compartment S ($\Delta_S = 1.2$), 30% undercounting in class I and Q ($\Delta_\ell = 0.7$ for $\ell = I, Q$) and 30% overcounting in compartment S ($\Delta_S = 1.3$), 50% undercounting in the infected and isolated compartments ($\Delta_\ell = 0.5$ for $\ell = I$ and Q) and 50%

Parameter	Description	Value	Reference
N_0	initial total population size (millions)	126	[11, 22]
I_0	the initial size of the infectious population (millions)	0.06	[10]
Q_0	the initial size of the isolated population (millions)	0.0001	[10]
R_0	the initial size of the recovered population (millions)	0.0001	[10]
S_0	the initial size of the susceptible population (millions)	$N_0 - I_0 - Q_0 - R_0$	[10]
$\hat{\beta}$	nominal transmission and contact in (2)	$\frac{0.126}{N_0}$	[19]
γ	recovery rate in (1)	0.03	[19]
τ	reciprocal of average isolation time in (1)	0.03	[19]
μ	nonassociative mortality in (1)	0.0000307	[11, 22]
B	immigration rate in (1)	3110×10^{-4}	[11, 22]
$\hat{\rho}$	nominal vaccination rate in (2)	0.00005	[10]
$\hat{\nu}$	nominal isolation rate in (2)	0.005	[10]
$\underline{\beta}$	tuning constant in $u_C(t)$ from (10)	$\frac{\hat{\beta}}{4}$	[10]
λ and χ	$\lambda = \gamma + \hat{\nu} + \mu$ and $\chi = \hat{\rho} + \mu$ used in equilibrium	-	[10]
ω_V	tuning parameter for control $u_V(t)$	0.000015	[10]
ω_I	tuning parameter for control $u_I(t)$	0.00006	[10]
ω_C	tuning parameter for control $u_C(t)$	0.0000001	[10]
c	constant from (4)	0.02	[10]
$c_\diamond$	constant from (4)	$1.8\bar{c}_\diamond$	[10]
$\bar{c}_\diamond$	bound (5) relating to tuning constant $c_\diamond$	$\frac{(\tau+\mu)c\lambda}{\hat{\nu}^2}$	[10]

TABLE 1. Parameter settings and descriptions when vaccination is present. These values were used in [10]. When no vaccination is present, the parameters are the same as in the table, except with $\omega_V = \hat{\rho} = 0$.

overcounting in class S ($\Delta_S = 1.5$), 70% undercounting in the infected and isolated compartments ($\Delta_\ell = 0.3$ for $\ell = I$ and Q) and 70% overcounting in class S ($\Delta_S = 1.7$), and 80% undercounting in the infected and isolated compartments ($\Delta_\ell = 0.2$ for $\ell = I$ and Q) and 80% overcounting in class S ($\Delta_S = 1.8$).

4. Measurement uncertainties applied to classes S, I, and Q that correspond to undercounting class I and Q and overcounting class S for varying percentage levels in the absence of vaccination, which correspond to choosing $\hat{\rho} = \omega_V = 0$ in the simulations. The percentage levels are 20% undercounting in class I and Q ($\Delta_\ell = 0.8$ for $\ell = I, Q$) and 20% overcounting in compartment S ($\Delta_S = 1.2$), 30% undercounting in class I and Q ($\Delta_\ell = 0.7$ for $\ell = I, Q$) and 30% overcounting in compartment S ($\Delta_S = 1.3$), 50% undercounting in the infected and isolated compartments ($\Delta_\ell = 0.5$ for $\ell = I,\ Q$) and 50 % overcounting in class S ($\Delta_S = 1.5$), 70% undercounting in the infected and isolated compartments ($\Delta_\ell = 0.3$ for $\ell = I,\ Q$) and 70% overcounting in class S ($\Delta_S = 1.7$), and 80% undercounting in the infected and isolated compartments ($\Delta_\ell = 0.2$ for $\ell = I,\ Q$) and 80% overcounting in class S ($\Delta_S = 1.8$).
5. Measurement uncertainties applied to classes S, I, and Q that correspond to overcounting in compartments S, I, and Q for varying percentage levels using

the values from Table 1. The percentage levels are 20% overcounting in class S, I, and Q ($\Delta_\ell = 1.2$ for $\ell = S,\ I,\ Q$), 30% overcounting in class S, I, and Q ($\Delta_\ell = 1.3$ for $\ell = S,\ I,\ Q$), 50% overcounting in compartments S, I, and Q ($\Delta_\ell = 1.5$ for $\ell = S,\ I,\ Q$), 70% overcounting in compartments S, I, and Q ($\Delta_\ell = 1.7$ for $\ell = S,\ I,\ Q$), and 80% overcounting in compartments S, I, and Q ($\Delta_\ell = 1.8$ for $\ell = S,\ I,\ Q$).

5.3.1. *Undercounting constant level of uncertainty results.* In Figure 3, we plot the states and controls corresponding to constant levels of measurement uncertainty due to undercounting in classes S, I, and Q. In Subfigures 3d, 3e, and 3f, the isolation control and the vaccination control rates are reduced dramatically when higher levels of uncertainty are assumed and the contact control is being prioritized. In Subfigure 3f, the behavior of each vaccination procedure is a decreasing function. In the case where no measurement uncertainty is applied (which is plotted by blue solid lines), the vaccination protocol is administered throughout time interval $[0, 500]$. As the undercounting percentages increase, the vaccination protocol is turned off sooner (meaning, u_V takes the value $u_V(t) = -\hat{\rho}$). In particular, in the case in which there is 50% undercounting (the purple dashed line) vaccination is turned off around day 180, and when there is 80% undercounting (the blue dashed line), vaccination is never activated.

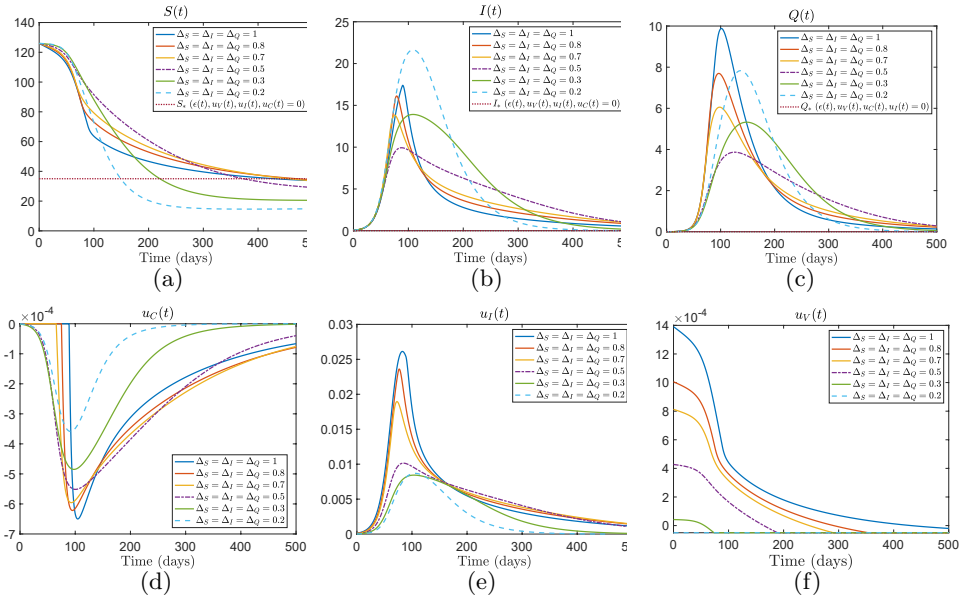

FIGURE 3. Constant levels of uncertainties due to undercounting in the S, I, and Q populations. The solid blue lines correspond to the case in which no undercounting occurs ($\Delta_\ell = 1$ for $\ell = S, I, Q$), the solid red lines correspond to 20% undercounting ($\Delta_\ell = 0.8$ for $\ell = S, I, Q$), the solid gold lines correspond to 30% undercounting ($\Delta_\ell = 0.7$ for $\ell = S, I, Q,$), the purple dash-dot lines correspond to 50% undercounting, the lime solid line corresponds to 70% undercounting, and the blue dash lines correspond to 80% undercounting.

In Subfigure 3d, we see that as the level of uncertainty due to undercounting increases, the contact control needs to be applied sooner. The blue solid line in Subfigure 3d is the feedback contact control in which no uncertainty measures are applied to the compartments. Here, the feedback control is activated around day 88. However, all of the other contact controls in Subfigure 3d are activated at earlier times. In cases where we assume that compartments S, I, and Q are underestimated by 50% (purple dash-dot line), by 70% (light green solid line), and by 80% (light blue dashed line), the contact control is applied within the first 20 days (albeit at very low levels) and the intensity of the contact control peaks around day 90 to day 100.

For the contact control corresponding to the 50% undercounting, the level of intensity of applying contact control peaks at a lower magnitude compared to the contact control in which there is not any uncertainty, and yet in Subfigure 3b we see (in the purple dash-dot line) that the infection peak is much lower compared to the peak infection that was generated by the feedback controls having no measurement uncertainty. Biologically speaking, this pertains to acting more quickly with nonpharmaceutical interventions (such as social distancing and mask usage) can "flatten the curve". Considering the susceptible population and the vaccination rate corresponding to the uncertainty measures set to being 0.5 (given by purple dash-dot lines in Subfigures 3a and 3f), the susceptible population remains high for the first 100 days because the contact control decreases their chances of becoming infected but also a large portion of the susceptible are not receiving long-term immunity through vaccination. Once the contact control starts to relax (near day 100), these susceptibles are now at risk of becoming infected. This explains Subfigure 3b where the infection class corresponding to 50% undercounting (purple dash-dot line) does not decrease towards zero as quickly compared to other cases. This illustrates the effects of constant undercounting of the compartments.

5.3.2. *Constant levels of uncertainty due to undercounting without vaccination.* We now examine the effects of constant levels of uncertainties due to undercounting but in the absence of vaccination. Therefore, in these simulations, we set $\hat{\rho} = \omega_V = 0$ as in Remark 4.4, which produces the constant vaccination rate $\rho(t) = 0$ as explained in Remark 4.4. The motivation behind these simulations is to represent a scenario in which only non-pharmaceutical interventions (such as social distancing, mask usage, contact tracing, and quarantine/isolation) can be applied. In Figure 4, we provide plots of the states and controls, and in Figure 5 we provide a comparison plot of the transmission functions associated with using constant undercounting uncertainties and with vaccination (on the left) versus the transmission functions that are obtained when no vaccination is administered (on the right). In comparing the plots of the contact control in the absence of vaccination (in Subfigure 4d) with the contact controls with vaccination (in Subfigure 3d), both behave very similarly. The main difference between the two is the peak intensity is larger in the contact controls in the absence of vaccine, in comparison to the peak intensities of the contact control with vaccination. For example, in the case in which no uncertainity is applied the transmission rate (which is indicated by the blue solid line in Subfigure 5a) $\beta(t)$ drops to 0.000350068 at day 104.4, while in the same case but in the absence of vaccination (represented by the blue solid line in Subfigure 5b) $\beta(t)$ drops to 0.000286686 on day 100.6. In the case in which vaccination is considered and undercounting is 20% (which is represented by the red line in Subfigure 5a), $\beta(t)$ drops to 0.000378254 on day 94.7, while in the same case but

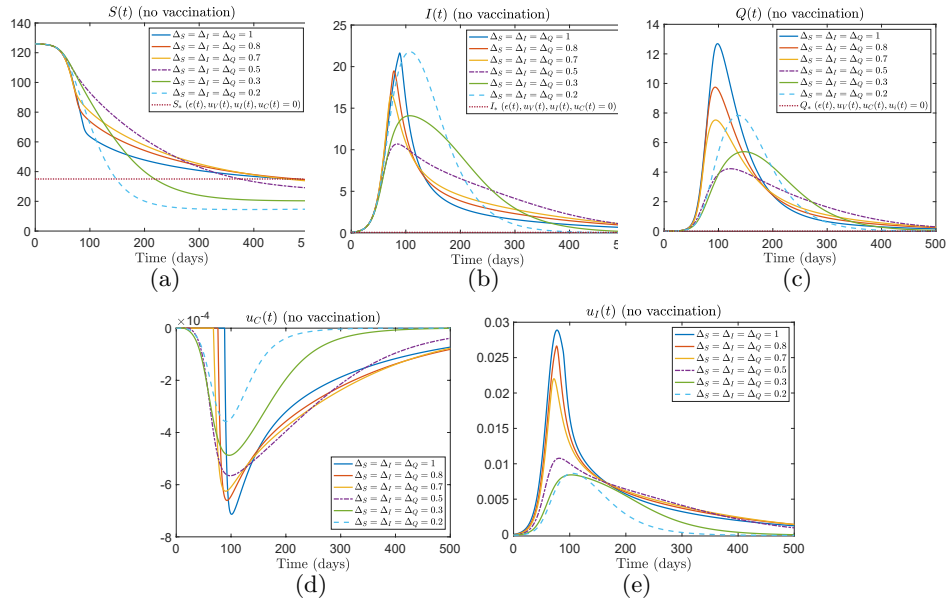

FIGURE 4. Constant levels of uncertainties due to undercounting in classes S, I, and Q without vaccination. The color and line style used represents the same levels of uncertainty as what was used in Figure 3.

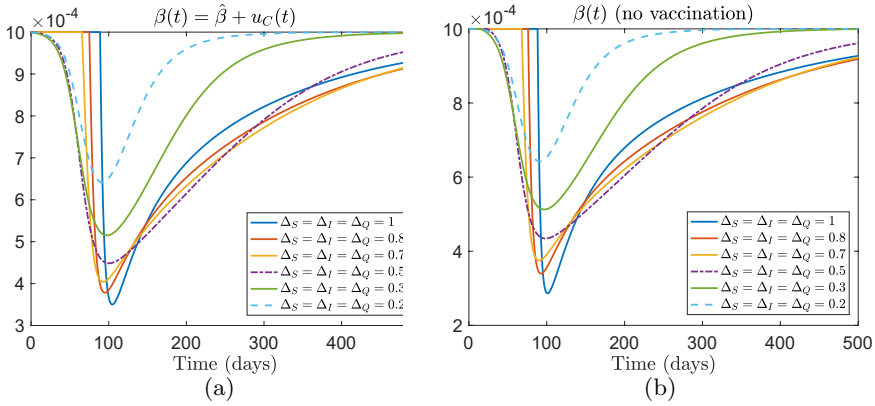

FIGURE 5. **Left.** Transmission rate with constant undercounting uncertainty measurements and with vaccination. **Right.** Transmission rate ($\beta(t) = \hat{\beta} + u_C(t)$) with constant undercounting uncertainty measurements and without vaccination. (Note: both subfigures are a vertical shift of the contact controls presented in Subfigures 3d and 4d).

with no vaccination applied (represented by the red line in Subfigure 5b), $\beta(t)$ drops to 0.000339657 on day 92. When pertaining to uncertainty measures that correspond to 50% undercounting or higher percentages of undercounting, these

changes in intensity are not really distinguishable. Regarding the isolation control with vaccination (Subfigure 3e) and without vaccination (Subfigure 4e), the overall behavior of the isolation controls remain the same, but the isolation controls peaks at a slightly larger rates when vaccination is not applied. The higher peaks are more noticeable in cases in which the levels of uncertainty are small, and become less pronounced when the percentage undercounting is very high. In the absence of vaccination, it makes sense to administer stricter measures that correspond to non-pharmaceutical interventions.

The more interesting characteristic corresponding to these simulations is in viewing how $I(t)$ changed due to no vaccination. With ρ set to being zero, the computed basic reproduction number is $\hat{R}_0 = 2.8918$. Consequently, we should expect increased peaks in $I(t)$. We compare the plots of the resulting state variable with all controls considered (given in Subfigure 3b) with the resulting state variable in which the vaccination is $\rho(t) = 0$ (given in Subfigure 4b). What we observed is that in cases in which undercounting is at high percentage levels, the change in the peak incidence is not as significant in comparison to what occurs when we have more certainty. In particular, in the case where no uncertainty measures is applied (which is represented by the solid blue line) the peak incidence is about 17.27 million people when vaccination is considered, but without vaccination the peak incidence is about 21.5 million. Similarly, when the compartments are undercounted by 20%, the peak incidence is approximately 16 million when vaccination is considered, but without vaccination the peak incidence jumps to about 19.3 million. When the percentage of undercounting of classes is 50%, the peak incidence is a little over 9.9 million when vaccination is considered, but without vaccination the peak incidence is approximately 10.68 million. We see little change in peak incidences in simulations where undercounting is larger than 50%. This is because the role of the contact control is prioritized more than vaccination in the case of high levels of undercounting. In cases where we were more certain, vaccination played a stronger role, so ignoring vaccination led to higher peaks in compartment I.

5.3.3. *Mixed constant levels of uncertainty.* We next provide simulations where the uncertainty for class S represents overcounting and the uncertainty for I and Q correspond to undercounting. Our motivation is that it is likely that those who are infectious but not counted as being infected could be incorrectly classified as susceptible. This can occur when considering asymptomatic individuals who do not get tested, or individuals who are infectious but get a false negative test result. We refer to the following simulations as mixed constant levels of uncertainty.

In Figure 6, we provide plots of the states and controls when incorporating mixed constant levels of uncertainty. In these simulations, the values of u_C and u_I in our formulas for the contact and isolation control are closer to zero as the uncertainty increases, and vaccination is being prioritized as we become more uncertain about each compartment. In Subfigure 6d, as the uncertainty due to undercounting I and Q and overcounting S increases, the contact control is activated later, and the intensity of that contact control decreases. In Subfigure 6e, the maximum of the isolation control decreases as the percentages of undercounting in I and Q and of overcounting in S increase. In the vaccination control u_V values in Subfigure 6f, the rate of vaccination is increased (at the start of the epidemic) as the percents of undercounting in I and Q and of overcounting in S increase. From a stability analysis standpoint, vaccination is being prioritized here to ensure that $S(t)$ approaches S_* (i.e., the endemic steady state value which is the red dotted line given

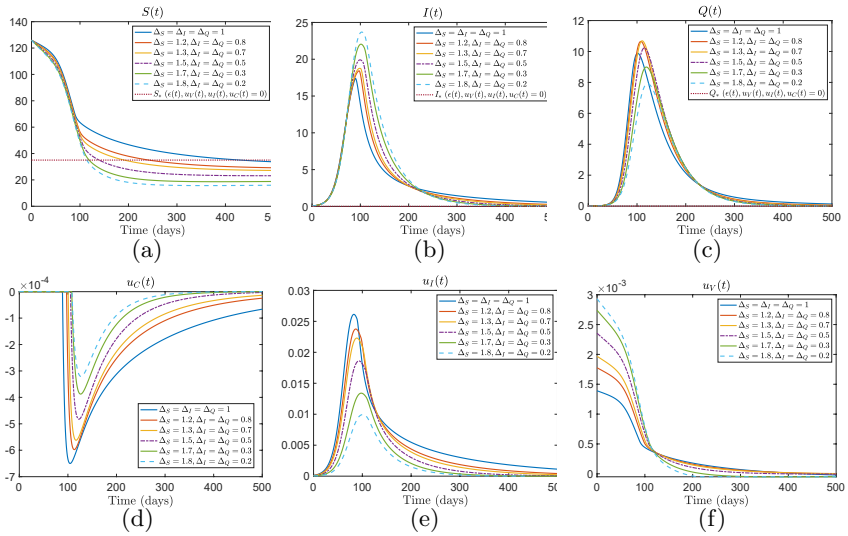

FIGURE 6. Mixed constant levels of uncertainty results due to undercounting I and Q and overcounting S. The solid blue lines correspond to the case in which no undercounting occurs ($\Delta_\ell = 1$ for $\ell = S, I, Q$), the solid red lines correspond to 20% undercounting in I and Q ($\Delta_\ell = 0.8$ for $\ell = I, Q$) and 20% overcounting in S ($\Delta_S = 1.2$). The solid gold lines correspond to 30% undercounting in I and Q ($\Delta_\ell = 0.7$ for $\ell = I, Q$) and 30% overcounting in S ($\Delta_S = 1.3$), the purple dash-dot lines correspond to 50% undercounting in I and Q ($\Delta_\ell = 0.5$ for $\ell = I, Q$) and 50% overcounting in S ($\Delta_S = 1.5$), the lime solid line corresponds to 70% undercounting in I and Q and 70% overcounting in S, and the blue dash lines correspond to 80% undercounting in I and Q and 80% overcounting in S.

in Subfigure 6a)) as t grows. The resulting feedback controls lead to increases in the peak incidence (as seen in Subfigure 6b) as we become more uncertain about the measurements for S, I, and Q.

5.3.4. *Mixed constant levels of uncertainty without vaccination.* We next provide simulations of mixed constant levels of uncertainty without vaccination, i.e., the case of Remark 4.4, where only non-pharmaceutical interventions can be applied. We set $\hat{\rho} = \omega_V = 0$ as in Remark 4.4, which produces the constant vaccination rate $\rho(t) = 0$ as explained in Remark 4.4. The computed basic reproduction number is approximately 2.8918. An increase in the basic reproduction number should lead to increased peak incidences. In Figure 7, the plots of the states and controls are provided. Comparing these results to those where vaccination is applied (in Figure 6), we see that the behaviors of the contact controls are similar, but the intensity for the control increased. Comparing the minimum values of u_C in Subfigure 6d to minimum values of the contact controls of u_C without vaccination (in Subfigure 7d), we see little change in values when we are more certain about S, I, and Q. However, when the uncertainty measurements corresponding to percentages of undercounting

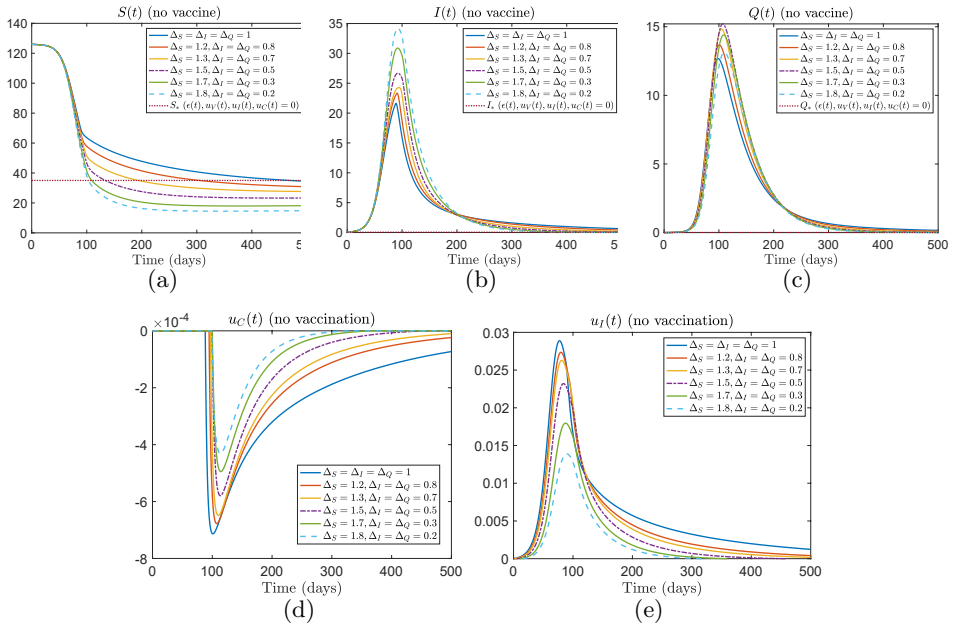

FIGURE 7. Constant uncertainties due to undercounting of I and Q and overcounting of S (without vaccination). The color and line style represents same levels of uncertainty as what was used in Figure 6.

in I and Q and of overcounting in S is 50% or larger, the corresponding contact controls drop to lower minima when vaccination is ignored.

Considering the isolation control in the absence of vaccination (in Subfigure 7e), we observe that the peak values of u_I are larger when vaccination is ignored in comparison to the peak values of u_I when vaccination is considered in Subfigure 6e. These changes are distinguishable regardless of what level of uncertainty is applied. This, and the changes in compartments $Q(t)$ (compared with Subfigures 6c with 7c), suggest that isolation plays a larger role when vaccination is unavailable and the susceptible population is overcounted; however, combining the isolation and contact controls has limited effects on reducing the peak incidence. Comparing Subfigure 6b with 4b, we see an increase in peak incidence when vaccination is not available.

5.3.5. *Constant level of uncertainty due to overcounting.* We provide simulations with constant uncertainty due to overcounting compartments S, I, and Q, and where vaccination is also being used, in Figure 8. Compared with the simulations for mixed overcounting and undercounting in Figure 6 where the only overcounting is for class S, the simulations when overcounting is present for all three variables in the controls are similar. This suggests that the impact of overcounting class S in Figure 6 is greater than than the combined impacts of undercounting classes I and Q in Figure 6, because changing from undercounting to overcounting in the classes I and Q had no significant impact.

5.4. **Time-varying measurement uncertainties from undercounting.** We next study time-varying uncertainty measurements of S, I, and Q to study how

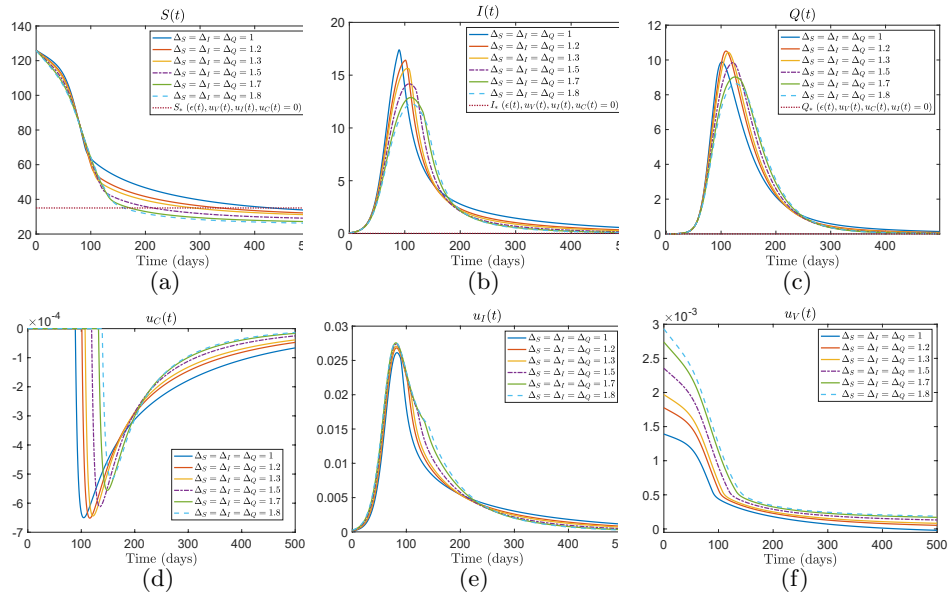

FIGURE 8. Constant uncertainties due to overcounting S, I, and Q. The solid blue lines correspond to the case with no uncertainty measurements ($\Delta_\ell = 1$ for $\ell = S, I, Q$), the red solid line corresponds to 20% overcounting of S, I, and Q ($\Delta_\ell = 1.2$ for $\ell = S,\ I,\ Q$), the solid gold line corresponds to 30% overcounting of S, I, and Q ($\Delta_\ell = 1.3$ for $\ell = S,\ I,\ Q$), the purple dash-dotted line corresponds to 50% overcounting of S, I, and Q ($\Delta_\ell = 1.5$ for $\ell = S,\ I,\ Q$), the solid lime colored lime corresponds to 70% overcounting of S, I, and Q ($\Delta_\ell = 1.7$ for $\ell = S,\ I,\ Q$), and blue dashed-line corresponds to 80% overcounting of S, I, and Q ($\Delta_\ell = 1.8$ for $\ell = S,\ I,\ Q$).

such measures (and the immigration perturbation) influence the behaviors of the controls and states. The first set of time-varying uncertainty measures are of the form similar to Hill functions. Our reason for this form is to represent a potential scenario in which the level of uncertainty decreases, which can occur during an epidemic as increased availability of resources (such as test kits and vaccines) can occur. The Hill functions investigated have a vertical shift included because $\Delta_I(t) \neq 0$ at any time. For $\ell = S, I, Q$, the uncertainty takes the form

$$\Delta_\ell(t) = \frac{(K_m - K_0)t^2}{H_0 + t^2} + K_0, \tag{34}$$

where K_0, K_m, and H_0 are constants. Here H_0 is the saturating constant (in all of our simulations H_0 =10,000), and $1-K_0$ is the initial percentage level of uncertainty due to undercounting (in all of our simulations K_0=0.2). As $t \to +\infty$, we get $\Delta_\ell(t) \to K_m$ for each i. This means that the percentage level of undercounting class ℓ (for $\ell = S, I$,and Q) is approaching $(1 - K_m)\%$. In our simulations we vary $K_m \in \{0.3, 0.4, 0.5, 0.7, 0.8, 1\}$, and in Subfigure 9a, we plot the Hill function uncertainties that we studied.

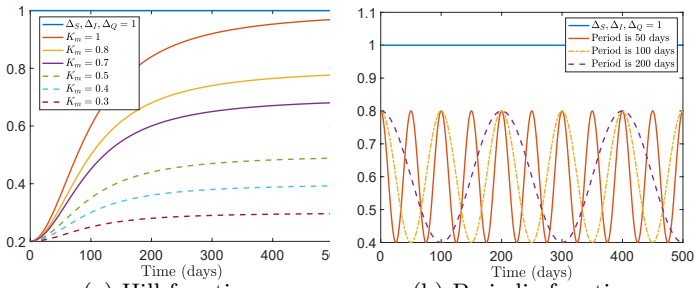

(a) Hill functions (b) Periodic functions

FIGURE 9. **Left.** Measurement uncertainties $\Delta_S = \Delta_I = \Delta_Q$ of the form of Hill functions (34) where $K_0 = 0.2$, $H_0 = 10,000$, and K_m is varied. **Right.** Plots of the periodic uncertainty measures.

We also investigate periodic time-varying uncertainty for varying periods. Our motivation is to consider timed events when a population's participation (in getting tested or vaccinated) fluctuates. The idea is that when individuals participate in testing and vaccination at higher levels of frequency, we have more accurate S, I, and Q counts. Increased population participation could occur in an event where a vaccine is approved to be administered for a specific age group, or near holidays, when individuals need to get tested and/or vaccinated to be approved for traveling. The periodic uncertainty functions are $\Delta_\ell(t) = 0.2\cos(2\pi t/p) + 0.6$ for $\ell = S$, I, and Q, where p is the period (in days). These uncertainty measurements fluctuate due to undercounting classes S, I and Q by 20% or undercounting the classes by 60%. For our simulations, we vary the period $p \in \{50, 100, 200\}$, and in Subfigure 9b, we provide plots of the periodic uncertainty measurements.

5.4.1. *Hill function and periodic uncertainty results.* We provide simulations where the measurement uncertainties are Hill functions or periodic, to illustrate Theorem 3.1, for the uncertainty functions in Figure 9. The values of the states and feedback controls are in Figures 10 and 11. In the simulations associated with using the Hill functions, each experiment begins with the assumption that the classes are undercounted by 80% but that the level of uncertainty is improved to where the level of undercounting for each class approaches $(1 - K_m)\%$ as $t \to +\infty$. When the uncertainties are Hill functions, the decrease in the susceptible population (in Subfigure 10a) was slower than the decreases in the susceptible population when there is constant overcounting or undercounting (in Figures 6a and 8a). This can be attributed to significant uncertainties at the start, which later have less effect. We observed similar slower reduction in the populations of infected individuals, but the peak infection levels were similar to the plots in Figures 6b and 8b for cases where the measurement uncertainties were constant. One difference between the plots is in the vaccination levels, where the vaccination levels for the Hill shaped uncertainty functions remained near zero for several choices of the Hill function parameters; see Figure 10f. This can be attributed to uncertainty in the population counts, resulting in more reliance on contact or isolation control.

In Subfigure 10b, as the percentage of undercounting is reduced (e.g., with $K_m = 0.7, 0.8$, and 1), the peak incidence is reduced significantly compared with the peak incidence corresponding to the feedback control that has no uncertainty (see solid

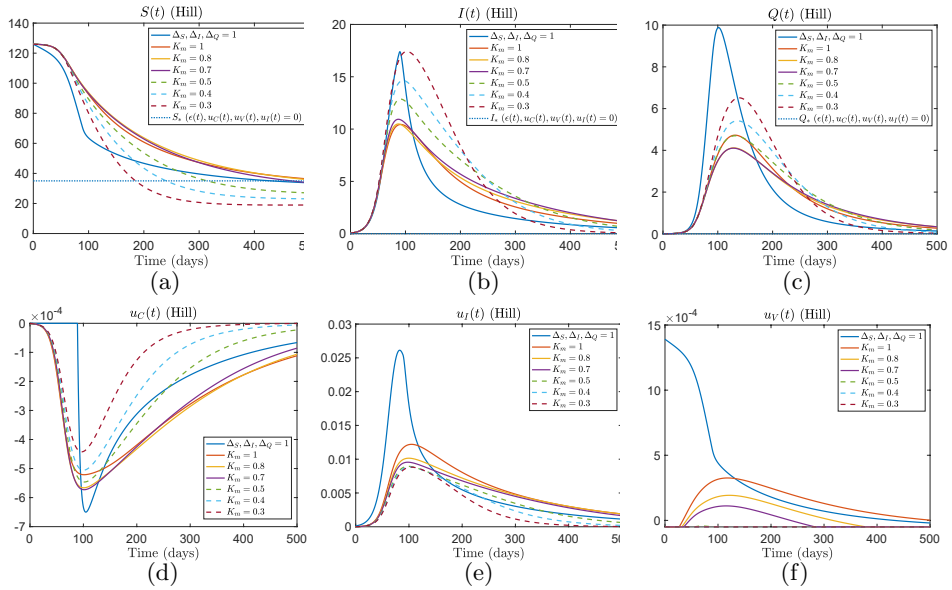

FIGURE 10. Uncertainties (in all classes) being Hill functions (plots of uncertainty measurements are in Subfigure 9a)

blue line). This suggests the usefulness of non-pharmaceutical interventions being applied early, when undercounting of the infectious populations is at high levels at the beginning of the epidemic. We observed a similar increase in settling times for S, I, and Q under periodic uncertainties, in Subfigures 11a-11c. Although the periodicity of the measurement uncertainties did not produce periodic oscillation of the states in Figures 11a-c, we see such oscillations in Figures 11d-11f. A notable difference between the vaccination control levels in the periodic case in Figure 11f and the Hill function case in Figure 10f is that, unlike the Hill function case, the periodic case called for positive vaccination levels early.

5.4.2. *Measurement uncertainties in Theorem 4.1.* Our final simulations correspond to cases where Δ_S, Δ_I, and Δ_Q are time-varying and satisfy the requirements of Theorem 4.1, where the uncertainty values are generated by solving the discretized optimization problem (33). The number of iterations needed to reach convergence is 21. In Figure 12, we see a trade-off that when the state is close to the equilibrium, the ranges of allowable uncertainty values that satisfy the requirement of Theorem 4.1 may be reduced, e.g., $\Delta_S(t)$ in Figure 12c must be chosen to be closer to 1. However, our requirements from Theorem 4.1 allowed $\Delta_I(t)$ and $\Delta_Q(t)$ values that were far from 1. In Figure 14, we compare the feedback control values that are generated without uncertainty with the values that arise using the uncertainty measurements that are generated by Theorem 4.1. In Figure 13 we plot the resulting states. The behaviors of the contact and isolation controls are similar in both cases, except for regions where the controls spike or drop when the measurement uncertainties spike or drop. This can be attributed to our feedback structures that depend on measurement uncertainties and state values (through products of uncertainty and state values), i.e., the controls react to the uncertainty by calling for more isolation.

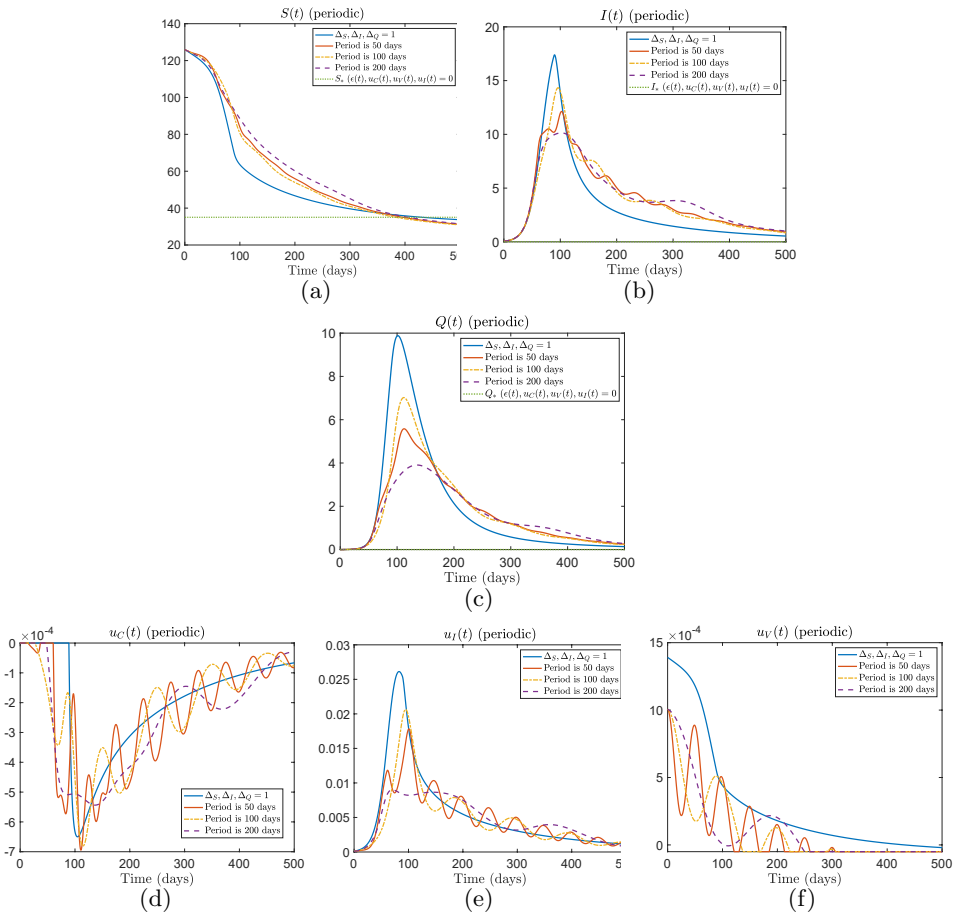

FIGURE 11. States and controls when periodic levels of uncertainties are in classes S, I and Q.

This contrasts significantly with standard optimal controls, which do not take the state or measurement uncertainties into account.

Comparing the feedback controls generated by the uncertainty measurements from Theorem 4.1 to the controls generated without uncertainty, we see that the uncertainty measurements contribute to generating a contact control that is activated sooner, an isolation control that has a lower peak intensity, and a vaccination control that involves lower rates of vaccination for the majority of the time interval. As shown in Figure 13, the feedback control strategy generated by Theorem 4.1 yields an increase in the peak incidence, which can be attributed to the uncertainties, which are largely compensated for by our feedback controls.

6. **Conclusions.** We advanced the state of the art in the study of

SIQR models, by developing new equal signs conditions that enabled us to quantify the effects of measurement uncertainties that arise from using feedback controls that ensure ISS. This contrasts with prior ISS studies of SIQR models, whose uncertainties were confined to being immigration uncertainties. Our multiplicative measurement uncertainties are amenable to modeling the effects of measurement

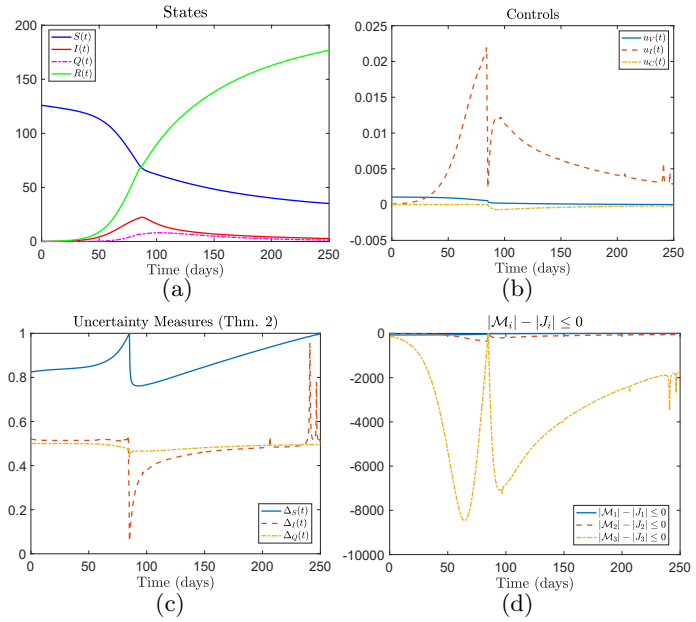

FIGURE 12. Results corresponding to Theorem 4.1. Subfigure (d) shows that the uncertainties satisfy condition (28).

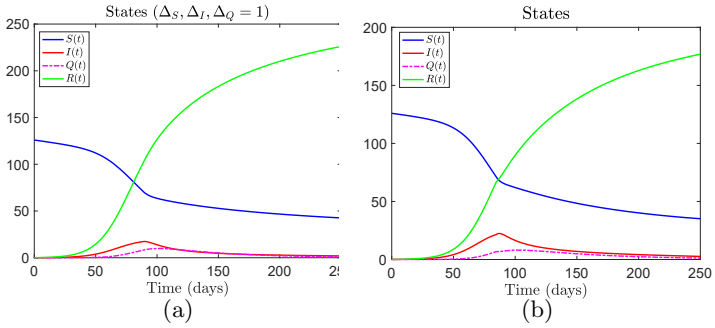

FIGURE 13. **Left.** Plot of the state solutions when applying the feedback controls in which no uncertainty is applied. **Right.** Plots of the state solutions when applying the feedback controls corresponding to Theorem 4.1.

delays, sampled measurements, and over- and under-counting of susceptible, infected, and quarantined individuals. We applied our approach using parameters that arose in the COVID-19 pandemic, by illustrating the effects of overcounting and undercounting. We hope to extend our analysis to cover delay compensating age-structured SIQR models, where instead of a system of ordinary differential equations, the dynamics would be a system of ordinary differential equations interconnected with a system of first order hyperbolic differential equations.

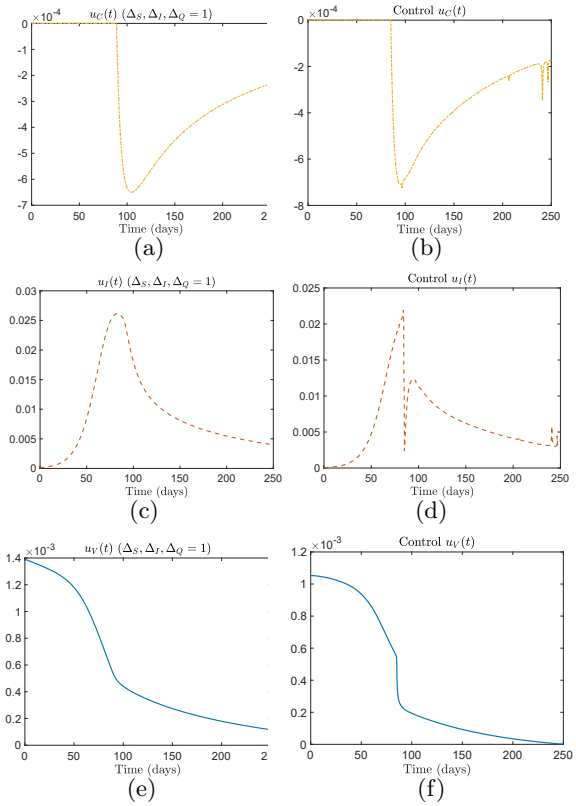

FIGURE 14. **Left.** The results corresponding to the feedback controls in which no uncertainty measures are applied. **Right.** The results corresponding to the feedback controls corresponding to Theorem 4.1.

Acknowledgments. The authors thank Prof. Maia Martcheva of the University of Florida Department of Mathematics, for helpful discussions that inspired this work.

REFERENCES

[1] G. Albi, L. Pareschi and M. Zanella, Modelling lockdown measures in epidemic outbreaks using selective socio-economic containment with uncertainty, *Mathematical Biosciences and Engineering*, **18** (2021), 7161-7190.

[2] R. Dutta, S. N. Gomes, D. Kalise and L. Pacchiardi, Using mobility data in the design of optimal lockdown strategies for the COVID-19 pandemic, *PLoS Computational Biology*, **17** (2021), e1009236.

[3] J. Franceschi, A. Medaglia and M. Zanella, On the optimal control of kinetic epidemic models with uncertain social features, *Optimal Control Applications and Methods*, 2023, to appear.

[4] H. Hethcote, M. Zhien and L. Shengbing, Effects of quarantine in six endemic models for infectious diseases, *Mathematical Biosciences*, **180** (2002), 141-160.

[5] H. Ito, A construction of strict Lyapunov functions for a bilinear balancing model, *IFAC-PapersOnLine*, **54** (2021), 161-166.

[6] H. Ito, Input-to-state stability and Lyapunov functions with explicit domains for SIR model of infectious diseases, *Discrete and Continuous Dynamical Systems-Series B*, **26** (2021), 5171-5196.

[7] H. Ito, Vaccination with input-to-state stability for SIR model of epidemics, In *Proceedings of the 60th IEEE Conference on Decision and Control*, 2021, 2812-2817.
[8] H. Ito, Isolation-oriented Lyapunov-based design of simultaneous feedback strategies for disease control of SIQR, *International Journal of Robust and Nonlinear Control*, **32** (2022), 8767-8785.
[9] H. Ito, M. Malisoff and F. Mazenc, Strict Lyapunov functions and feedback controls for SIR models with quarantine and vaccination, *Discrete and Continuous Dynamical Systems-Series B*, **27** (2022), 6969-6988.
[10] H. Ito, M. Malisoff and F. Mazenc, Feedback control of isolation and contact for SIQR epidemic model via strict Lyapunov function, *Mathematical Control and Related Fields*, **13** (2023), 1438-1465.
[11] Japanese Ministry of Health, Labour and Welfare, COVID-19 latest information, 2023, https://www.mhlw.go.jp/english/.
[12] M. Keeling and P. Rohani, *Modeling Infectious Diseases in Humans and Animals*, Princeton University Press, Princeton, NJ, 2008.
[13] H. Khalil, *Nonlinear Systems*, Third Edition, Prentice Hall, Englewood Cliffs, NJ, 2002.
[14] A. Korobeinikov, Lyapunov functions and global stability for SIR and SIRS epidemiological models with non-linear transmission, *Bulletin of Mathematical Biology*, **68** (2006), 615-626.
[15] A. Korobeinikov and P. Maini, A Lyapunov function and global properties for SIR and SEIR epidemiological models with nonlinear incidence, *Math. Biosci. Eng.*, **1** (2004), 57-60.
[16] A. Korobeinikov and G. C. Wake, Lyapunov functions and global stability for SIR, SIRS, and SIS epidemiological models, *Applied Mathematics Letters*, **15** (2002), 955-960.
[17] S. Lenhart and J. T. Workman, *Optimal Control Applied to Biological Models*, Chapman and Hall/CRC, London, UK, 2007.
[18] M. Malisoff and F. Mazenc, *Constructions of Strict Lyapunov Functions*, Springer Science & Business Media, New York, NY, 2009.
[19] T. Odagaki, Analysis of the outbreak of COVID-19 in Japan by SIQR model, *Infectious Disease Modelling*, **5** (2020), 691-698.
[20] M. Sadeghi, J. M. Greene and E. D. Sontag, Universal features of epidemic models under social distancing guidelines, *Annual Reviews in Control*, **51** (2021), 426-440.
[21] E. Sontag, Input to state stability: Basic concepts and results, In P. Nistri and G. Stefani, editors, *Nonlinear and Optimal Control Theory*, Springer, Berlin, Germany, 2008, 163-220.
[22] Statistics Bureau Of Japan, Monthly Report, 2023, https://www.stat.go.jp/.
[23] S. Tang, Y. Xiao and D. Clancy, New modelling approach concerning integrated disease control and cost-effectivity, *Nonlinear Analysis: Theory, Methods & Applications*, **63** (2005), 439-471.
[24] C. Tian, Q. Zhang and L. Zhang, Global stability in a networked SIR epidemic model, *Applied Mathematics Letters*, **107** (2020), 106444, 6 pp.
[25] G. G. Walter and M. Contreras, *Compartmental Modeling with Networks*, Springer Science & Business Media, New York, NY, 1999.

Received March 2023; revised October 2023; early access December 2023.